HHS Public Access

Author manuscript

Nature. Author manuscript; available in PMC 2020 October 22.

Published in final edited form as:

Nature. 2020 May ; 581(7807): 199–203. doi:10.1038/s41586-020-2210-3.

Ligand-induced BIK1 monoubiquitination regulates plant immunity

Xiyu Ma[1,2], **Lucas A. N. Claus**[3,4], **Michelle E. Leslie**[5,*,^], **Kai Tao**[6,*], **Zhiping Wu**[7,*], **Jun Liu**[1,2], **Xiao Yu**[2,8], **Bo Li**[2,8], **Jinggeng Zhou**[1,2], **Daniel V. Savatin**[3,4], **Junmin Peng**[7], **Brett M. Tyler**[6], **Antje Heese**[5], **Eugenia Russinova**[3,4], **Ping He**[1,2,#], **Libo Shan**[2,8,#]

[1]Department of Biochemistry and Biophysics, Texas A&M University, College Station, TX 77843, USA

[2]Institute for Plant Genomics and Biotechnology, Texas A&M University, College Station, TX 77843, USA

[3]Department of Plant Biotechnology and Bioinformatics, Ghent University, 9052 Ghent, Belgium

[4]Center for Plant Systems Biology, VIB, 9052 Ghent, Belgium

[5]Department of Biochemistry, Interdisciplinary Plant Group, University of Missouri-Columbia, Columbia, Missouri 65211, USA

[6]Center for Genome Research and Biocomputing and Department of Botany and Plant Pathology, Oregon State University, Corvallis, Oregon 97331, USA

[7]Departments of Structural Biology and Developmental Neurobiology, Center for Proteomics and Metabolomics, St. Jude Children's Research Hospital, Memphis, TN 38105, USA

[8]Department of Plant Pathology and Microbiology, Texas A&M University, College Station, TX 77843, USA

Abstract

Recognition of microbe-associated molecular patterns (MAMPs) via plasma membrane (PM)-resident pattern recognition receptors (PRRs) triggers the first line of inducible defense against invading pathogens[1–3]. Receptor-like cytoplasmic kinases (RLCKs) are convergent regulators that

[#]**Corresponding authors**: Ping He, pinghe@tamu.edu, Libo Shan, lshan@tamu.edu, Institute for Plant Genomics and Biotechnology, Texas A&M University.

[^]Current address: Elemental Enzymes, 1685 Galt Industrial Blvd, St. Louis, MO, 63132, United States

Author contributions X.M., P.H. and L.S. conceived and designed the experiments; X.M. performed most of molecular, biochemical and transgenic experiments; L.A.N.C. and D.V.S., under the supervision of E.R, conducted BIK1, BIK1^{9KR} and FLS2 endocytosis experiments in the transgenic plants and *N. benthamiana*, colocalization with ARA6, and spatial and temporal dynamics of BIK1 and FLS2 endocytosis in *N. benthamiana*; M.E.L., under the supervision of A.H., performed BIK1 and FLS2 endocytosis in transgenic plants by spinning disc confocal microscopy; K.T., under the supervision of B.T., conducted BIK1^{G2A} localization, BIK1 endocytosis and colocalization with ARA6 experiments in *N. benthamiana*; Z.W., under the supervision of J.P., identified BIK1 *in vivo* and *in vitro* ubiquitination sites with LC-MS/MS; J.L. performed Co-IP and *Botrytis* infection assays; X.Y. performed Co-IP and transgenic plant assays; B.L. generated *35S::BIK1-GFP* transgenic plants; J.Z. performed *in vitro* kinase assays; E.R., A.H., B.T., and J.P. analyzed data, provided critical feedback and helped shape the research. All experiments were independently reproduced in different laboratories. X.M., P.H. and L.S. wrote the manuscript with inputs from all authors.

[*]These authors contribute equally.

Competing interests The authors declare no competing interests.

associate with multiple PRRs in plants[4]. The mechanisms underlying PM-tethered RLCK activation remain elusive. We report here that, upon MAMP perception, RLCK *BOTRYTIS*-INDUCED KINASE 1 (BIK1) is monoubiquitinated following phosphorylation, then released from the flagellin receptor FLAGELLIN SENSING 2 (FLS2)-BRASSINOSTEROID INSENSITIVE 1-ASSOCIATED KINASE 1 (BAK1) complex, and internalized dynamically into endocytic compartments. Arabidopsis E3 ubiquitin ligases RING-H2 FINGER A3A (RHA3A) and RHA3B mediate the monoubiquitination of BIK1, which is essential for the subsequent BIK1 release from the FLS2-BAK1 complex and immune signaling activation. Ligand-induced monoubiquitination and endosomal puncta of BIK1 exhibit spatial and temporal dynamics distinct from those of PRR FLS2. Our study reveals the intertwined regulation of PRR-RLCK complex activation by protein phosphorylation and ubiquitination, and elucidates that ligand-induced monoubiquitination contributes to the release of BIK1 family RLCKs from the PRR complex and activation of PRR signaling.

Prompt activation of PRRs upon microbial infection is essential for hosts to defend against pathogen attacks[1–3]. The arabidopsis BIK1 family RLCKs are immune regulators associated with multiple PRRs, including the bacterial flagellin receptor FLS2, and co-receptor BAK1/SERKs[5,6]. Upon ligand perception, BIK1 is phosphorylated by BAK1 and subsequently dissociates from the FLS2-BAK1 complex[7]. Downstream of the PRR complex, BIK1 phosphorylates PM-resident NADPH oxidases to regulate reactive oxygen species (ROS) production[8,9], and cyclic nucleotide-gated channels to trigger a rise of cytosolic calcium[10]. However, it remains elusive how BIK1 activation and dynamic association with the PRR complex is regulated.

Ligand-induced increase of BIK1 puncta

We observed that BIK1-GFP localized to both the periphery of epidermal pavement cells and intracellular puncta using arabidopsis transgenic plants expressing functional *35S::BIK1-GFP* by spinning disc confocal microscopy (SDCM) (Fig. 1a, Extended Data Fig. 1a, b). BIK1-GFP colocalized with the FM4–64-stained PM (Fig. 1b, star), and frequently within endosomal compartments (Fig. 1b, arrowheads). Time-lapse SDCM shows that BIK1-GFP puncta were highly mobile, disappearing (red circle), appearing (yellow circle), and moving rapidly in and out of the plane of view (white circle) (Extended Data Fig. 1c). The abundance of BIK1-GFP puncta was increased over time (3–17 and 18–32 min) after treatment with flagellin peptide flg22 (Fig. 1c; Extended Data Fig. 1d–p). The timing of the ligand-induced increase in BIK1-GFP puncta differed from that of FLS2-GFP, in which puncta numbers were significantly increased 35 min after flg22 treatment (Fig. 1d)[11–13]. Ligand-induced endocytosis of FLS2 contributes to the degradation of the activated FLS2 receptor and attenuation of the signaling[11–14], whereas increased abundance of BIK1-GFP puncta precedes that of FLS2-GFP (Fig. 1c, d).

Ligand-induced BIK1 monoubiquitination

Ligand-induced FLS2 degradation is mediated by U-box E3 ligases PUB12 and PUB13 that polyubiquitinate FLS2[15–17]. We tested whether BIK1 is ubiquitinated upon flg22 treatment with an *in vivo* ubiquitination assay in arabidopsis protoplasts co-expressing FLAG epitope-

tagged ubiquitin (FLAG-UBQ) and HA epitope-tagged BIK1 (Fig. 1e; Extended Data Fig. 2a). The results showed that flg22 treatment induced BIK1 ubiquitination (Fig. 1e), as ubiquitinated BIK1 was detected with an α-HA immunoblot upon immunoprecipitation with an α-FLAG antibody. The flg22-induced BIK1 ubiquitination was also observed in *pBIK1::BIK1-HA* transgenic plants (Extended Data Fig. 2b). The strong and discrete band of ubiquitinated BIK1 indicates monoubiquitination (Fig. 1e; Extended Data Fig. 2a, b) compared to polyubiquitination of BAK1 and FLS2 with a ladder-like smear of protein migration (Extended Data Fig. 2c, d). The apparent molecular mass of ubiquitinated BIK1 (~52 kDa) is ~8 kDa larger than that of unmodified BIK1 (44 kDa), supporting the attachment of a single ubiquitin to BIK1. Incubation with the catalytic domain of the deubiquitinase Usp2 (Usp2-cc), but not its heat-inactivated form, reduced the molecular mass by ~8 kDa (Fig. 1e). In addition, a similar ubiquitination pattern of BIK1 was observed when we used the UBQ^{K0} variant, in which all seven lysine (K) residues in UBQ were changed to arginine (R), thus preventing polyubiquitination chain formation (Extended Data Fig. 2e, f). Notably, flg22-induced BIK1 ubiquitination was blocked by treatment with the ubiquitination inhibitor PYR-41, but not by the proteasome inhibitor MG132, and was not observed in the *fls2* or *bak1–4* mutants (Extended Data Fig. 2g–i). In addition to flg22, other MAMPs, including elf18, pep1, and chitin, also induced monoubiquitination of BIK1 (Extended Data Fig. 2j), in line with the notion that BIK1 is a convergent component downstream of multiple PRRs[4]. Monoubiquitination of the BIK1 family RLCKs PBL1 and PBL10, but not another RLCK BSK1, was enhanced upon flg22 treatment (Extended Data Fig. 2k, l), suggesting that MAMP perception induces monoubiquitination of BIK1 family RLCKs.

Upon flg22 perception, BIK1 is phosphorylated, as detected by an immunoblot mobility shift within 1 min, with a plateau around 10 min (Fig. 1f)[5]. However, flg22-induced BIK1 ubiquitination becomes apparent only at 10 min after treatment and reaches a plateau around 30 min (Fig. 1f), suggesting that flg22-induced BIK1 ubiquitination may occur after its phosphorylation. Consistently, BIK1 phosphorylation deficient mutants, including a kinase-inactive mutant ($BIK1^{KM}$) and two phosphorylation site mutants ($BIK1^{T237A}$ and $BIK1^{Y250A}$) largely compromised flg22-induced ubiquitination (Fig. 1g). In addition, the kinase inhibitor K252a blocked flg22-induced BIK1 ubiquitination (Extended Data Fig. 3a). Moreover, PM localization is required for BIK1 ubiquitination as $BIK1^{G2A}$, a mutation at the myristoylation motif essential for PM localization, was unable to be ubiquitinated upon flg22 treatment (Extended Data Fig. 3b, c). Taken together, these data suggest that flg22-induced BIK1 phosphorylation is a prerequisite for its monoubiquitination at the PM.

BIK1 ubiquitination by RHA3A and RHA3B

There are 30 lysine residues in BIK1, all of which could potentially be ubiquitinated. We individually mutated 28 lysine residues to arginine except K105/K106 (located in the ATP-binding pocket and required for kinase activity), and screened for flg22-induced ubiquitination. None of the individual K-to-R mutants blocked BIK1 ubiquitination without altering its kinase activity (Extended Data Fig. 3d). $BIK1^{K204R}$, which compromised flg22-induced BIK1 monoubiquitination, also showed reduced phosphorylation *in vivo* and *in vitro* (Extended Data Fig. 3d, e). To identify BIK1-associated regulators, we carried out a

yeast two-hybrid screen using BIK1^{G2A} as a bait, and identified *RHA3A* (*AT2G17450*) encoding a functionally uncharacterized E3 ubiquitin ligase with a RING-H2 finger domain and an N-terminal transmembrane domain (Fig. 2a). We confirmed the interaction of BIK1 with RHA3A using an *in vitro* pull-down assay (Fig. 2b), an *in vivo* co-immunoprecipitation (Co-IP) assay in arabidopsis protoplasts (Extended Data Fig. 4a), and Co-IP in transgenic plants expressing both genes under their native promoters (Fig. 2c; Extended Data Fig. 4b). RHA3B, encoded by *AT4G35480*, the closest homolog of RHA3A bearing 66% amino acid identity (Fig. 2a), also co-immunoprecipitated with BIK1 (Extended Data Fig. 4c). Flg22 treatment did not affect BIK1 interaction with RHA3A or RHA3B (called RHA3A/B henceforth) (Extended Data Fig. 4a, c). Moreover, RHA3A/B co-immunoprecipitated with FLS2 (Extended Data Fig. 4d).

An *in vitro* ubiquitination assay demonstrated that RHA3A had autoubiquitination activity and monoubiquitinated itself (Extended Data Fig. 5a, b). Importantly, glutathione-*S*-transferase (GST)-RHA3A, but not GST-RHA3A^{I104A} with substitution of a conserved isoleucine (I) residue, monoubiquitinated GST-BIK1-HA as evidenced by an additional discrete band that migrated ~8kD larger (Fig. 2d). The available *rha3a* and *rha3b* T-DNA insertion lines did not show significant reduction of the corresponding transcripts (Extended Data Fig. 5c). We thus generated artificial microRNAs (amiRNAs) of *RHA3A/B*[18], and co-expression of *amiR-RHA3A* and *amiR-RHA3B*, but not *amiR-RHA3A* alone, suppressed flg22-induced BIK1 monoubiquitination in protoplast transient assays (Extended Data Fig. 5d, e). Flg22-induced BIK1 monoubiquitination, but not phosphorylation, was also reduced in transgenic plants expressing *amiR-RHA3A* and *amiR-RHA3B* driven by the native promoters (Extended Data Fig. 5f, g). Furthermore, we generated *rha3a* and *rha3a/b* mutants using the CRISPR/Cas9 system (Extended Data Fig. 5h). Flg22-induced BIK1 monoubiquitination was reduced in *rha3a/b* (Fig. 2e). The data together indicate that RHA3A/B modulate flg22-induced BIK1 monoubiquitination.

RHA3A-mediated BIK1 ubiquitination sites

To identify RHA3A-mediated BIK1 ubiquitination sites, we performed liquid chromatography-tandem mass spectrometry (LC-MS/MS) analysis of *in vitro* ubiquitinated BIK1. Among ten lysine residues identified (Fig. 3a, b; Extended Data Fig. 6a–i), K^{106} residing in the ATP-binding pocket blocked BIK1 kinase activity when mutated[7]. Among the other nine lysine sites, all six lysine (K95, K170, K186, K286, K337, and K358) with available structural information are located on the BIK1 surface (Fig. 3c)[19]. Furthermore, six ubiquitinated lysine residues were detected by LC-MS/MS of *in vivo* ubiquitinated BIK1-GFP upon flg22 treatment, and they all overlap with those detected in *in vitro* RHA3A-BIK1 ubiquitination reactions (Extended Data Fig. 7a–h). Individual lysine mutations did not affect BIK1 ubiquitination *in vivo* (Extended Data Fig. 3d), whereas combined mutations of the N-terminal five lysine (BIK1^{N5KR}) or C-terminal four lysine (BIK1^{C4KR}) partially compromised flg22-induced BIK1 ubiquitination, and BIK1^{9KR} with all nine lysine mutated largely blocked flg22-induced BIK1 monoubiquitination *in vivo* (Fig. 3d) and RHA3A-mediated *in vitro* ubiquitination (Fig. 3e). BIK1^{9KR} exhibited similar activities as BIK1 with regard to its *in vitro* kinase activities (Fig. 3f), flg22-induced BIK1 phosphorylation, and association with RHA3A in protoplasts (Extended Data Fig. 8a, b). Furthermore,

35S::BIK1^{9KR}*-HA/*WT transgenic plants had normal flg22-induced MAPK activation and ROS production (Extended Data Fig. 8c, d). Collectively, the data indicate that RHA3A monoubiquitinates BIK1 and that BIK1 phosphorylation does not require monoubiquitination. Notably, BIK1 monoubiquitination may not be restricted to a single lysine, and multiple lysine residues could serve as monoubiquitin conjugation sites. Alternatively, monoubiquitination might be the primary form of BIK1 modification, whereas polyubiquitinated BIK1 could be short-lived.

BIK1 monoubiquitination in immunity

BIK1^{9KR}, which eliminates BIK1 monoubiquitination but not phosphorylation, enabled us to examine the function of BIK1 monoubiquitination without compromised kinase activity. We generated *BIK1*^{9KR} transgenic plants driven by the *BIK1* native promoter in *bik1* (*pBIK1::BIK1*^{9KR}*-HA/bik1*) (Extended Data Fig. 8e, f). Unlike *pBIK1::BIK1-HA/bik1* transgenic plants, *pBIK1::BIK1*^{9KR}*-HA/bik1* transgenic plants exhibited a reduced flg22-triggered ROS burst similar to the *bik1* mutant (Fig. 4a). Moreover, *pBIK1::BIK1*^{9KR}*-HA/bik1* transgenic plants were more susceptible to the bacterial pathogen *Pseudomonas syringae* pv. *tomato* (*Pst*) DC3000 *hrcC*$^{-}$ compared to wild-type (WT) or *pBIK1::BIK1-HA/bik1* transgenic plants (Fig. 4b). In addition, *amiR-RHA3A/B* transgenic plants exhibited compromised flg22-triggered ROS production and enhanced susceptibility to *Pst* DC3000 (Fig. 4c, d) and *Pst* DC3000 *hrcC*$^{-}$, and to the fungal pathogen, *Botrytis cinerea* (Extended Data Fig. 8g, h). Similar results were obtained with the *rha3a/b* mutants (Extended Data Fig. 8i, j). Together, the data indicate that RHA3A/B-mediated monoubiquitination of BIK1 plays a role in regulating ROS production and plant immunity.

BIK1 monoubiquitination in endocytosis

Since perception of flg22 moderately increased the BIK1-GFP positive endosomal puncta (Fig. 1c), we tested whether BIK1 monoubiquitination is involved in flg22-triggered BIK1 endocytosis. Apparently, fewer FM4–64-labelled puncta were observed with BIK1^{9KR}-GFP than with BIK1-GFP after 10 or 15 min flg22 treatment (Extended Data Fig. 9a, b). In addition, we compared the flg22-triggered endocytosis of BIK1-TagRFP and BIK1^{9KR}-TagRFP co-expressing FLS2-YFP in *Nicotiana benthamiana*. Similar to transgenic plants (Fig. 1c, d), endosomal puncta of BIK1-TagRFP increased at 10–20 min, whereas FLS2-YFP puncta increased only after 60 min flg22 treatment (Fig. 4e, f; Extended Data Fig. 9c). A large portion (~90%) of flg22-induced BIK1-TagRFP puncta did not co-localize with FLS2-YFP puncta (Extended Data Fig. 9d), suggesting that BIK1 and FLS2 are likely not internalized together. This is in line with different ubiquitination characteristics of BIK1 and FLS2 (mono vs. poly, 10 min vs. 1 hr). In contrast to BIK1, BIK1^{9KR}-TagRFP was more abundant in puncta before treatment, but the number of puncta did not increase after flg22 treatment (Fig. 4e, f; Extended Data Fig. 9c), indicating that BIK1^{9KR}-TagRFP internalization does not respond to PRR activation. In addition, colocalization of BIK1^{9KR}-TagRFP with ARA6-YFP, a plant specific Rab GTPase residing on late endosomes[20], was significantly reduced when compared to that of BIK1-TagRFP (Extended Data Fig. 9e, f). Notably, flg22-induced FLS2-YFP endocytosis was absent in the presence of BIK1^{9KR}-TagRFP (Fig. 4e, f). Altogether, our data support the conclusion that ligand-induced BIK1

monoubiquitination contributes to its internalization from PM. Interestingly, whereas flg22 treatment induced a phosphorylation-dependent BIK1 dissociation from FLS2[5,6,21], flg22-triggered BIK1 dissociation from FLS2 was largely absent in the case of BIK1^{9KR} (Fig. 4g), which is consistent with the data that BIK1^{9KR} impaired FLS2 internalization (Fig. 4e, f). In addition, we observed an increased association between BIK1^{9KR} and FLS2 without flg22 treatment (Fig. 4g). Treatment with the ubiquitination inhibitor PYR-41 also blocked flg22-induced BIK1 dissociation from FLS2 and enhanced BIK1-FLS2 association (Extended Data Fig. 10a). Our data indicate that ligand-induced BIK1 monoubiquitination plays an important role in BIK1 dissociation from the PM-localized PRR complex, its endocytosis and immune signaling activation (Extended Data Fig. 10b).

Discussion

The BIK1 family RLCKs are central players in plant PRR signaling with many layers of regulation[4,22]. BIK1 stability is critical to maintain immune homeostasis. Plant U-box proteins PUB25 and PUB26 polyubiquitinate BIK1 and regulate its stability in the steady state[23]. This module only regulates non-activated BIK1 homeostasis without affecting ligand-activated BIK1[23]. Our study identified a role of RHA3A/B in monoubiquitinating BIK1 and activating PRR signaling, which is distinct from that of PUB25/26. BIK1^{9KR} protein levels in transgenic plants and protoplasts are comparable with BIK1 (Extended Data Fig. 10c, d), suggesting that BIK1 monoubiquitination may not regulate its stability. The nature of protein ubiquitination, including monoubiquitination and polyubiquitination, dictates distinct fates of substrates, such as proteasome-mediated protein degradation, nonproteolytic functions of protein kinase activation, and membrane trafficking[24]. Ligand-induced polyubiquitination of FLS2 by PUB12/13 promotes FLS2 degradation, thereby attenuating immune signaling[15,16], whereas ligand-induced monoubiquitination of BIK1 triggers BIK1 dissociation from PRR complexes and intracellular signaling activation. Thus, differential ubiquitination and endocytosis of distinct PRR-RLCK complex components likely serve as cues to fine-tune plant immune responses.

METHODS

Plant materials and growth conditions

Arabidopsis thaliana accession Col-0 (wild type, WT), mutants *fls2*, *bak1–4*, *bik1*, transgenic *pBIK1::BIK1-HA* in the *bik1* background, and *pFLS2::FLS2-GFP* in the Col-0 background were described previously[7,13]. *p35S::BIK-GFP* and *p35S::BIK1^{9KR}-GFP* in the Col-0 background, *pBIK1::BIK1^{9KR}-HA* transgenic plants in the *bik1* background, *p35S::BIK1-HA*, *p35S::BIK1^{9KR}-HA* transgenic plants in the Col-0 background, *pBIK1::BIK1-HA* in the Col-0 background, *pBIK1::BIK1-HA/ pRHA3A::RHA3A-FLAG* double transgenic plants in the Col-0 background and *pRHA3A::amiR-RHA3A-pRHA3B::amiR-RHA3B* transgenic plants in the Col-0 background were generated in this study (see below for details). All arabidopsis plants were grown in soil (Metro Mix 366, Sunshine LP5 or Sunshine LC1, Jolly Gardener C/20 or C/GP) in a growth chamber at 20–23°C, 50% relative humidity and 75 μE $m^{-2}s^{-1}$ light with a 12-hr light/12-hr dark photoperiod for four weeks before pathogen infection assay, protoplast isolation, and ROS

assay. For confocal microscopy imaging, seeds were sterilized, maintained for 2 days at 4°C in the dark, and germinated on vertical half-strength Murashige and Skoog (1/2 MS) medium [1% (wt/vol) sucrose] agar plates, pH 5.8, at 22°C in a 16-hr light/8-hr dark cycle for 5 days with a light intensity of 75 μE m^{-2} s^{-1}. For FM4–64 staining, whole seedlings were incubated for 15 min in 3 ml of 1/2 MS liquid medium containing 2 μM FM4–64, washed twice by dipping into deionized water before adding the elicitors (flg22, 100 nM). Wild-type tobacco (*N. benthamiana*) plants were grown under 14 h of light and 10 hr of darkness at 25 °C.

Statistical analyses

Data for quantification analyses are presented as mean ± standard error of mean (SEM). The statistical analyses were performed by Student's *t*-test or one-way analysis of variance (ANOVA) test. Number of replicates is shown in the figure legends.

Plasmid construction and generation of transgenic plants

FLS2, BAK1, BIK1, PBL1, PBL10 or BSK1 tagged with HA, FLAG or GFP in a plant gene expression vector pHBT used for protoplast assays, and $FLS2^{CD}$, $BAK1^{CD}$, $BAK1^{K}$, PUB13, BIK1, or $BIK1^{KM}$ fused with GST or MBP used for *E. coli* fusion protein isolation were described previously[5,7]. BIK1 point mutations in *pHBT* vector were generated by site-directed mutagenesis with primers listed in the Supplemental Table 1 (Table S1) using the *pHBT-BIK1-HA* construct as the template. $BIK1^{N5KR}$ was constructed by sequentially mutating K41, K95, K170 and K186 into arginine on $BIK1^{K31R}$. $BIK1^{C4KR}$ was constructed by sequentially mutating K337, K358 and K366 on $BIK1^{K286R}$. *pHBT-*$BIK1^{N5KR}$ and *pHBT-*$BIK1^{C4KR}$ were then digested with XbaI and StuI and ligated together to generate *pHBT-*$BIK1^{9KR}$*-HA*. $BIK1^{9KR}$ was sub-cloned into *pHBT-FLAG* or *pHBT-GFP* with BamHI and StuI digestion to generate *pHBT-*$BIK1^{9KR}$*-FLAG* or *pHBT-*$BIK1^{9KR}$*-GFP*. $BIK1^{9KR}$ was sub-cloned into the binary vector *pCB302-pBIK1::BIK1-HA* or *pCB302–35S::BIK1-HA* with BamHI and StuI digestion to generate *pCB302-pBIK1::*$BIK1^{9KR}$*-HA*, or *pCB302–35S::*$BIK1^{9KR}$*-HA*. *BIK1-GFP* or $BIK1^{9KR}$*-GFP* was sub-cloned into *pCB302* with BamHI and PstI digestion to generate *pCB302–35S::BIK1-GFP* and *pCB302–35S::*$BIK1^{9KR}$*-GFP*. $BIK1^{K204R}$, or $BIK1^{9KR}$ was sub-cloned into a modified GST (*pGEX4T-1*, Pharmacia) vector with BamHI and StuI digestion to generate *pGST-*$BIK1^{K204R}$, and *pGST-*$BIK1^{9KR}$ respectively. *BIK1-HA* or $BIK1^{9KR}$*-HA* was further sub-cloned into the *pGST* vector as following: digestion with PstI, blunting end by T4 DNA polymerase, digestion with BamHI and ligation into a BamHI/StuI digested *pGST* vector to generate *pGST-BIK1-HA* and *pGST-*$BIK1^{9KR}$*-HA*.

The *RHA3A* gene (*AT2G17450*) was cloned by PCR amplification from Col-0 cDNAs with primers containing BamHI at the 5' end and StuI at the 3' end, followed by BamHI and StuI digestion and ligation into the *pHBT* vector with an HA or FLAG tag at the C-terminus. The *RHA3B* gene (*AT4G35480*) was cloned similarly as *RHA3A* using BamHI and SmaI-containing primers. The *pHBT-*$RHA3A^{I104A}$ was generated by site-directed mutagenesis with primers listed in the Supplemental Table 1. The $RHA3A^{CD}$ (amino acid 50–186) or $RHA3A^{CD/I104A}$ were cloned by PCR amplification from *RHA3A* or $RHA3A^{I104A}$ with BamHI and StuI-containing primers. $RHA3A^{CD}$ and $RHA3A^{CD/I104A}$ were sub-cloned into

pGST or a modified *pMBP* (pMAL-c2, NEB) vector with BamHI and StuI digestion for *E. coli* fusion protein isolation. The promoter of *RHA3A* or *RHA3B* was PCR-amplified from genomic DNAs of Col-0 with primers containing SacI and BamHI, and ligated into *pHBT*. The fragment of *pRHA3A::RHA3A-FLAG* was digested by SacI and EcoRI, and ligated into *pCAMBIA2300*.

Artificial mircoRNA (amiRNA) constructs were generated as previously described[18]. In brief, amiRNA candidates were designed according to the website http://wmd3.weigelworld.org/cgi-bin/webapp.cgi. Three candidates were chosen for each gene with *RHA3A* for *amiRNA480*: TTTTGTCAATACACTCCACGG; *amiRNA211*: TCAACGCAGATAAGAGCGCTA; *amiRNA109*: TCAAGTAATCTTGACGGTCGT, and *RHA3B* for *amiRNA444*: TTATGCATATTGCACACTCCG; *amiRNA113*: TAATCTAGAGGAGCGAGTCAG; *amiRNA214*: TCTACGCATACGAGAGCGCAT. Primers for cloning amiRNAs were generated according to the wmd3 website (http://wmd3.weigelworld.org/cgi-bin/webapp.cgi). The cognate fragments were cloned into the *pHBT-amiRNA-ICE1* vector[18]. The *pCB302-pRHA3A::amiRNA-RHA3A-pRHA3B::amiRNA-RHA3B* was constructed as following: the promoter of *RHA3A* was PCR amplified from *pRHA3A::RHA3A-FLAG*, digested with SacI and BamHI and ligated with *pHBT-amiR-RHA3A* to generate *pHBT-pRHA3A::amiR-RHA3A*. The *pRHA3A::amiR-RHA3A* fragment was further released by SacI and PstI digestion and ligated into pCB302 vector to generate *pCB302-pRHA3A::amiRNA-RHA3A*. The *pHBT-pRHA3B::amiR-RHA3B* was constructed similarly followed by PCR amplification using primer containing SacI sites at both the 5' and 3'ends, subsequent digestion with SacI and ligation into the *pCB302-pRHA3A::amiRNA-RHA3A* vector. Tandem *pRHA3A/B-amiRNA-RHA3A/B* in the same direction was confirmed by digestion and selected for further experiments.

The *rha3a/b* mutant was generated by the CRISPR/Cas9 system following the published protocol[25]. Briefly, primers containing guide RNA (gRNA) sequences of *RHA3A* and *RHA3B* were used in PCR to insert both gRNA sequences into the *pDT1T2* vector. The *pDT1T2* vector containing both gRNAs was further PCR amplified, digested with BsaI and ligated into a binary vector *pHEE401E*. *Agrobacterium tumefaciens*-mediated floral dip was used to transform the *pHEE401E* vector into Col-0 plants. Genomic DNAs from hygromycin (25 μg/ml) positive plants were extracted, PCR amplified with gene-specific primers and sequenced by Sanger sequencing.

The monomer ubiquitin of arabidopsis ubiquitin gene 10 (*UBQ10*, *At4g05320*) carrying lysine-to-arginine mutations at all the seven lysine residues (UBQ^{K0}: 5'-ATGCAGATCTTTGTTAGGACTCTCACCGGAAGGACTATCACCCTCGAGGTGGAAAGCTCTGACACCATCGACAACGTTAGGGCCAGGATCCAGGATAGGGAAGGTATTCCTCCGGATCAGCAGAGGCTTATCTTCGCCGGAAGGCAGTTGGAGGATGGCCGCACGTTGGCGGATTACAATATCCAGAGGGAATCCACCCTCCACTTGGTCCTCAGGCTCCGTGGTGGTTAA-3') was synthesized and cloned into a *pUC57* vector by GenScript USA Incorporation. UBQ^{K0} was then amplified by PCR with primers listed in the Table S1 and further sub-cloned into a modified *pHBT* vector with BamHI and PstI digestion to generate *pHBT-FLAG-*UBQ^{K0}.

Plasmids used for the transient expression in *N. benthamiana* were constructed as reported previously[26]. Briefly, *FLS2*, *BIK1*, and *BIK1*^{9KR} were PCR amplified and recombined into a *pDONR207-YFP*, *pDONR207-TagRFP*, and *pDONR207-GFP* vector by In-Fusion® HD Cloning (TaKaRa Bio). The *pDONR207* vectors were subsequently transferred to a destination vector *pmAEV* (derived from binary vector *pCAMBIA* with a 35S promoter) using the Gateway® LR reaction (Thermo Fisher scientific lnc.).

DNA fragments cloned into the final constructs were confirmed via Sanger sequencing. *Agrobacterium tumefaciens*-mediated floral dip was used to transform the above binary vectors into *bik1* or Col-0 plants. The transgenic plants were selected by Glufosinate-ammonium (Basta, 50 μg/ml) for the *pCB302* vector or kanamycin (50 μg/ml) for the *pCAMBIA2300* vector. Multiple transgenic lines were analyzed by immunoblot (IB) for protein expression. Two lines with 3:1 segregation ratios for antibiotic resistance in the T3 generation were selected to obtain homozygous seeds for further studies. The *amiR-RHA3A/B* transgenic plants resistant to Basta in T2 generation were used for assays.

Yeast two-hybrid screen

The cDNA library constructed in a modified pGADT7 vector (Clontech) was previously described[15]. BIK1^{G2A} from *pHBT-BIK1*^{G2A}*-HA* was sub-cloned into a modified *pGBKT7* vector with BamHI and StuI digestion. *pGBK-BIK1*^{G2A} was transformed into the yeast AH109 strain. The resulting yeast transformants were then transformed with the cDNA library and screened in the synthetic defined media (SD) without Trp, Leu, His, Ade (SD-T-L-H-A) and SD-T-L-H containing 1 mM 3-amino-1, 2, 4-triazole (3-AT). The confirmed yeast colonies were subjected to plasmid isolation and sequencing.

Pathogen infection assays

Pseudomonas syringae pv. *tomato* (*Pst*) DC3000 was cultured overnight at 28°C in the King's B medium supplemented with rifamycin (50 μg/ml). Bacteria were collected by centrifugation at 3,000 g, washed and re-suspended to the density of 10^6 cfu/ml with 10 mM $MgCl_2$. Leaves from four-week-old plants were hand-inoculated with bacterial suspension using a needleless syringe. To measure *in planta* bacterial growth, five to six sets of two leaf discs of 6 mm in diameter were punched and grounded in 100 μl of ddH_2O. Serial dilutions were plated on TSA plates (1% tryptone, 1% sucrose, 0.1% glutamatic acid and 1.8% agar) containing 25 μg/ml rifamycin. Plates were incubated at 28°C and bacterial colony forming units (cfu) were counted 2 days after incubation. For spray inoculation, *Pst* DC3000 or *Pst* DC3000 *hrcC*$^-$ bacteria were collected and re-suspended to 5×10^8 cfu/ml with 10 mM $MgCl_2$, silwet L-77 (0.02%) and sprayed onto leaf surface. Plants were covered with a transparent plastic dome to keep humidity after spray. After incubation, the 3rd pair of true leaves was detached, soaked in 70% ethanol for 30 seconds, rinsed in water and bacterial growth was measured similarly as above.

Protoplast transient expression and co-immunoprecipitation (Co-IP) assays

Protoplast isolation and transient expression assay have been described previously[27]. For protoplast-based Co-IP assay, protoplasts were transfected with a pair of constructs (the empty vectors as controls, 100 μg DNA for 500 μl protoplasts at the density of 2×10^5/ml

for each sample) and incubated at room temperature for 6–10 hr. After treatment of flg22 with indicated concentration and time points, protoplasts were collected by centrifugation and lysed in 300 μl Co-IP buffer (150 mM NaCl, 50 mM Tris-HCl, pH7.5, 5 mM EDTA, 0.5% Triton, 1 × protease inhibitor cocktail, before use, adding 2.5 μl 0.4 M DTT, 2 μl 1 M NaF and 2 μl 1 M Na_3VO_3 for 1 ml IP buffer) by vortexing. After centrifugation at 10,000 g for 10 min at 4°C, 30 μl of supernatant was collected for input controls and 7 μl of α-FLAG-agarose beads were added into the remaining supernatant and incubated at 4 °C for 1.5 hr. Beads were collected and washed three times with washing buffer (150 mM NaCl, 50 mM Tris-HCl, pH7.5, 5 mM EDTA, 0.5% Triton) and once with 50 mM Tris-HCl, pH7.5. Immunoprecipitates were analyzed by IB with indicated antibodies. The amiRNA candidate screens were performed as previously described[18].

In vivo ubiquitination assay

FLAG-tagged UBQ (FLAG-UBQ) or a vector control (40 μg DNA) was co-transfected with the target gene with an HA tag (40 μg DNA) into 400 μl protoplasts at the density of 2×10^5/ml for each sample and protoplasts were incubated at room temperature for 6–10 hr. After treatment with 100 nM flg22 at the indicated time points, protoplasts were collected for Co-IP assay in Co-IP buffer containing 1% Triton X-100. PYR-41 (Sigma, Cat # N2915) was added at the indicated concentrations and time points in the figure legends.

Recombinant protein isolation and *in vitro* kinase assays

Fusion proteins were produced from *E. coli* BL21 at 16°C using LB medium with 0.25 mM isopropyl β-D-1-thiogalactopyranoside (IPTG). Glutathione S-transferase (GST) fusion proteins were purified with Pierce glutathione agarose (Thermo Scientific), and maltose binding protein (MBP) fusion proteins were purified using amylose resin (New England Biolabs) according to the standard protocol from companies. The *in vitro* kinase assays were performed with 0.5 μg kinase proteins and 5 μg substrate proteins in 30 μl kinase reaction buffer (10 mM Tris-HCl, pH7.5, 5 mM $MgCl_2$, 2.5 mM EDTA, 50 mM NaCl, 0.5 mM DTT, 50 μM ATP and 1 μCi [γ $-^{32}$P] ATP). After gentle shaking at room temperature for 2 hr, samples were denatured with 4 × SDS loading buffer and separated by 10% SDS-PAGE gel. Phosphorylation was analyzed by autoradiography.

In vitro ubiquitination assay

Ubiquitination assays were performed as previously described with modifications[28]. Reactions containing 1 μg of substrates, 1 μg of HIS_6-E1 (AtUBA1), 1 μg of HIS_6-E2 (AtUBC8), 1 μg of GST-E3, 1 μg of ubiquitin (Boston Biochem, Cat # U-100AT-05M) in the ubiquitination reaction buffer (20 mM Tris-HCl, pH 7.5, 5 mM $MgCl_2$, 0.5 mM DTT, 2 mM ATP) were incubated at 30°C for 3 hr. The ubiquitinated proteins were detected by IB with indicated antibodies. The rabbit monoclonal α-RHA3A antibody was generated according to company's standard protocol against the peptide: AGGDSPSPNKGLKKC (GenScript, USA).

In vitro deubiquitination assay

Mouse Usp2-cc was cloned by PCR amplification from mouse cDNAs with primers containing BamHI at the 5' end and SmaI at the 3' end, followed by BamHI and SmaI digestion and ligation into the *pGST* vector to construct *pGST-Usp2-cc*. GST-Usp2-cc fusion proteins were produced in *E. coli* BL21, and purified with Pierce glutathione agarose (Thermo Scientific) according to the standard protocol from company. Deubiquitination (DUB) assays were performed as previously described with modifications[29]. Briefly, an *in vitro* ubiquitination assay was performed overnight at 28°C as described above. The reaction was aliquoted into individual tubes containing Usp2-cc or heat-inactivated (HI) (95°C for 5 min) Usp2-cc as a control in the DUB reaction buffer (50 mM Tris-HCl, pH 7.5, 50 mM NaCl and 5 mM DTT) and incubated at 28°C for 5 hr. Samples were then denatured and analyzed by immunoblotting.

For *in vitro* DUB assay with flg22-induced ubiquitinated BIK1, BIK1-HA and FLAG-UBQ were expressed in arabidopsis protoplasts treated with 100 nM flg22 for 30 min. The ubiquitinated BIK1-HA proteins were immunoprecipitated as described above. After washing with 50 mM Tris-HCl, agarose beads were washed once with DUB dilution buffer (25 mM Tris-HCl, pH 7.5, 150 mM NaCl and 10 mM DTT) and mixed with GST-Usp2-cc in DUB reaction buffer. After overnight incubation, beads were denatured in SDS buffer and analyzed by immunoblotting.

MAPK assay

Five eleven-day-old arabidopsis seedlings per treatment grown on vertical plates with 1/2 MS medium were transferred into water for overnight before flg22 treatment. Seedlings were collected, drilled and lysed in 100 μl Co-IP buffer. Protein samples with 1 × SDS buffer were separated in 10% SDS-PAGE gel to detect pMPK3, pMPK6 and pMPK4 by IB with α-pERK1/2 antibody (Cell Signaling, Cat# 9101).

Detection of ROS production

The 3rd or 4th pair of true leaves from 4- to 5-week-old soil-grown arabidopsis plants were punched into leaf discs with the diameter of 5 mm. Leaf discs were incubated in 100 μl of ddH_2O with gentle shaking overnight. Water was replaced with 100 μl of reaction solution containing 50 μM luminol, 10 μg/ml horseradish peroxidase (Sigma-Aldrich) supplemented with or without 100 nM flg22. Luminescence was measured with a luminometer (GloMax®-Multi Detection System, Promega) with a setting of 1 min as the interval for a period of 40–60 min. Detected values of ROS production were indicated as means of Relative Light Units (RLU).

In vitro GST pull-down assay

GST or GST-BIK1 agarose beads were obtained after elution and washed with 1 × PBS (137 mM NaCl, 2.7 mM KCl, 15 mM Na_2HPO_4, 4.4 mM KH_2PO_4) for three times. HA tagged MBP-RHA3A^{CD} or MBP proteins (2 μg) were pre-incubated with 10 μl of prewashed glutathione agarose beads in 300 μl pull-down incubation buffer (20 mM Tris-HCl, pH 7.5, 100 mM NaCl, 0.1 mM EDTA, and 0.2% Triton X-100) for 30 min at 4°C. 5 μl of GST or GST-BIK1 agarose beads were pre-incubated with 20 μg of Bovin Serum Albumin (BSA,

Sigma, Cat # A7906) in 300 μl incubation buffer for 30 min at 4°C with gentle shaking. The supernatant containing MBP-RHA3A^{CD} or MBP was incubated with pre-incubated GST or GST-BIK1 agarose beads for 1 hr at 4°C with gentle shaking. The agarose beads were precipitated and washed three times in pull-down wash buffer (20 mM Tris-HCl, pH 7.5, 300 mM NaCl, 0.1 mM EDTA, and 0.5% Triton X-100). The pulled-down proteins were analyzed by IB with an α-MBP antibody (Biolegend, Cat # 906901).

Mass spectrometry analysis of ubiquitination sites

The *in vitro* ubiquitination reactions with GST-RHA3A^{CD} and GST-BIK1 or GST-BIK1^{K204R} were performed as mentioned above with overnight incubation. Reactions were loaded on an SDS-PAGE gel (7.5%) and ran for a relatively short time untill the ubiquitinated bands can be separated from the original GST-BIK1 (GST-BIK1 band ran less than 0.5 cm from the separating gel). Ubiquitinated bands were sliced, trypsin digested before LC-MS/MS analysis on an LTQ-Orbitrap hybrid mass spectrometer (Thermo Fisher) as previously described[30]. The MS/MS spectra were analyzed with SEQUEST software, and images were exported from SEQUEST.

In vivo BIK1 ubiquitination sites were identified as following: 20 ml of WT arabidopsis protoplasts with a concentration of 2 ×10^5 per ml were transfected with BIK1-GFP and FLAG-UBQ and the protoplasts were treated with 200nM flg22 for 30 min after 7 hr incubation. GFP-trap-Agarose beads (Chromotek, Cat # gta-20) were incubated with cell lysates in the ratio of 10 μl beads per 4 ×10^5 cells for 1 hr at 4°C and beads were pooled from 10 tubes, washed using IP buffer for 3 times, and denatured in SDS buffer. Samples were separated by 10% SDS-PAGE and stained with GelCode Blue Stain Reagent (Thermo Fisher Cat # 24590). Ubiquitinated bands were sliced and analyzed as mentioned above.

Confocal microscopy and image analysis

For the laser scanning confocal microscopy, images were taken using a Leica SP8X inverted confocal microscope equipped with a HC PL APO CS2 40×/1.10 and 63×/1.20 water-corrected objective. The excitation wavelength was 488 nm for both GFP, and FM4–64 (ThermoFisher T13320), 514 nm for YFP and 555 nm for TagRFP by using the white light laser. Emission was detected at 500–530 nm for GFP, 570–670 nm for FM4–64, 519–549 nm for YFP, and 569–635 nm for TagRFP by using Leica hybrid detectors. Autofluorescence was removed by adjusting the time gate window between 0.8 and 6 ns. Intensities were manipulated with the ImageJ software.

For spinning disc confocal microscopy (SDCM), image series were captured using a custom Olympus IX-71 inverted microscope (Center Valley, PA) equipped with a Yokogawa CSU-X1 5000 rpm spinning disc unit (Tokyo, Japan) and 60x-silicon oil objective (Olympus UPlanSApo 60x/1.30 Sil) as previously described[11]. For the custom SDCM system, GFP and FM4–64 were excited with a 488-nm diode laser and fluorescence was collected through a series of Semrock Brightline 488-nm single-edge dichroic beamsplitter and bandpass filters: 500–550 nm for GFP, and 590–625 nm for FM4–64. Camera exposure time was set to 150 msec. For each image series, 67 consecutive images at a z-step interval of 0.3 μm (20 μm total depth) were captured using Andor iQ2 software (Belfast, United Kingdom). Images

captured by custom SDCM were processed with the Fiji distribution of ImageJ 1.51 (https://fiji.sc/) software, and BIK1-GFP and FLS2-GFP endosomal puncta were quantified as number of puncta per 1000 μm^2 as previously described[11,31], with the exception that puncta were detected within a size distribution of 0.1–2.5 μm^2. For colocalization of BIK1-GFP with FM4–64 by custom SDCM, cotyledons were stained with 2.5 μM FM4–64 for 10 min, washed twice, and imaged after a 5-min chase.

For quantification of flg22-induced BIK1-GFP and BIK1^{9KR}-GFP-containing endosomal puncta over time, the maximum number of FM4–64 labeled spots per image area was set to 100%, and the percentage of GFP-colocalizing spots per time interval relative to the maximum was calculated; 20–25 images per time interval, captured from 5 individual plants per genotype were used for quantification.

For transient expression in *N. benthamiana, Agrobacterium* strain C58 carrying the constructs of interest was co-infiltrated in the abaxial side of tobacco leaves as described previously[32]. 48–72 hr after infiltration, multiple infiltrated leaves were infiltrated with 100 μM flg22 and imaged at the indicated time points. The number of puncta per 1000 μm^2 was quantified as previously described[11,31]. The percentage of BIK1 and FLS2 colocalization was calculated by dividing the number of BIK1-FLS2 colocalizing puncta by the total number of BIK1 puncta. The BIK1-ARA6 percentage of colocalization was calculated by dividing the number of BIK1-ARA6 or BIK1^{9KR}-ARA6 colocalizing puncta by the total number of ARA6 puncta.

qRT-PCR analysis

Total RNA was isolated from leaves of four-week-old plants with TRIzol reagent (Invitrogen). One μg of total RNA was treated with RNase-free DNase I (New England Biolabs) followed by complementary DNA (cDNA) synthesis with M-MuLV reverse transcriptase (New England Biolabs) and oligo(dT) primer. qRT-PCR analysis was performed using iTaq SYBR green Supermix (Bio-Rad) with primers listed in Supplemental Table 1 in a Bio-Rad CFX384 Real-Time PCR System. The expression of *RHA3A* and *RHA3B* was normalized to the expression of *ACTIN2*.

Data availability

The data supporting the findings of this study are available within the paper and its Supplementary Information files. Source Data (gels and graphs) for Figs. 1–4 and Extended Data Figs. 1–10 are provided with the paper.

Extended Data

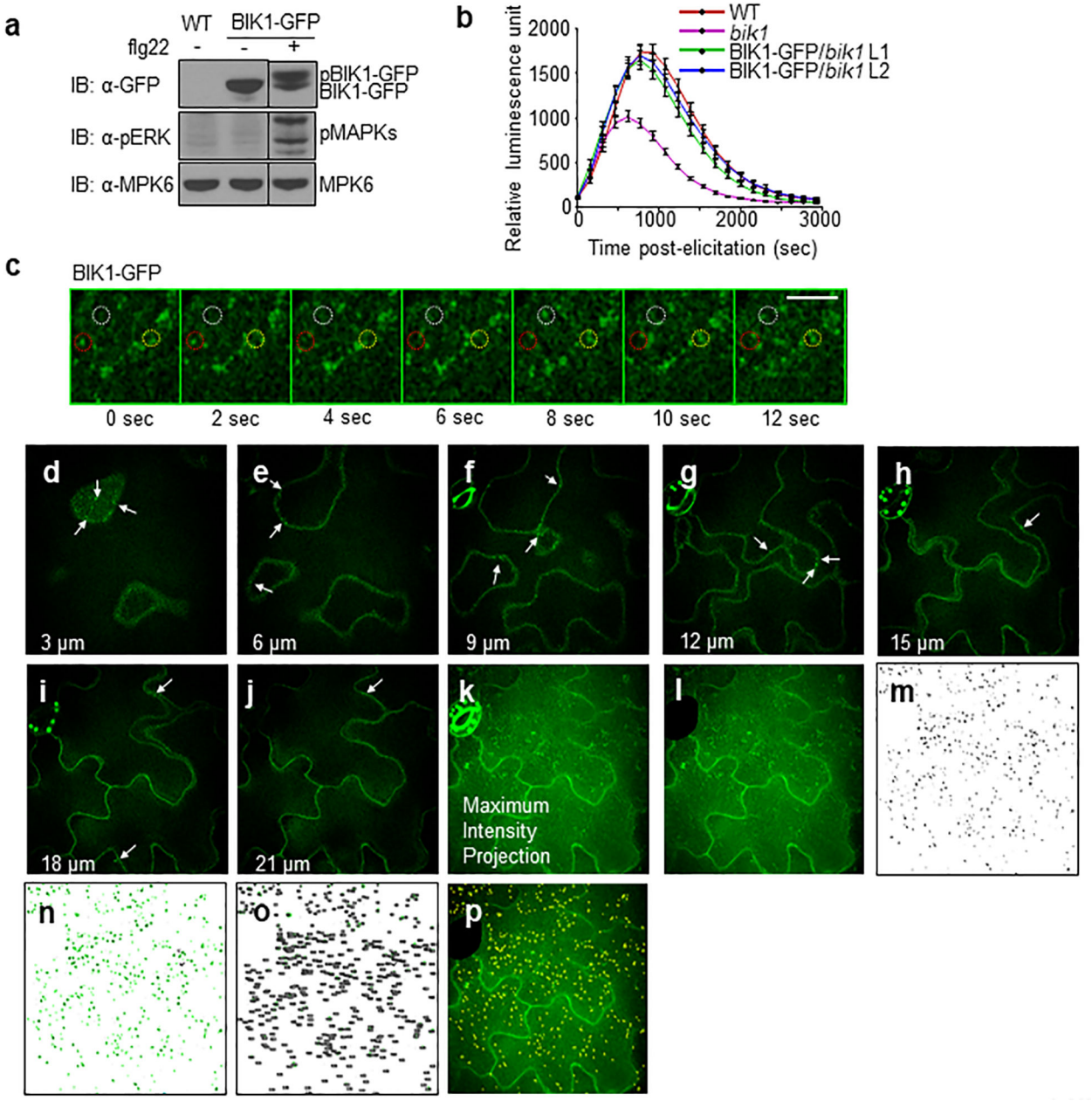

Extended Data Figure 1. BIK1-GFP is functional in plants and undergoes endocytosis.

a. BIK1-GFP is functional as confirmed by BIK1 phosphorylation in *35S::BIK1-GFP* expressing Col-0 cotyledons after 1 μM flg22 treatment. MPK6 is a loading control and the black stippled line indicates discontinuous segments from the same gel. **b**. BIK1-GFP restored ROS production in *bik1* upon flg22 treatment. Leaf discs from WT, *bik1* and BIK1-GFP complementation (Line 1 and 2) were treated with 100 nM flg22 for ROS measurement using a luminometer over 50 min. Data are shown as means ± SEM (WT, *bik1*: $n = 42$; BIK1-GFP/*bik1* $n = 45$). **c**. Time-lapse SDCM shows that BIK1-GFP endosomal puncta are highly mobile with puncta that disappear (red circle), appear (yellow circle), and rapidly move in and out of the plane of view (white circle). Scale bar, 5 μm. **d**-**k**. BIK1-GFP

localizes to endosomal puncta and PM in cross-sectional images of epidermal cells. The abaxial epidermal cells of cotyledons expressing BIK1-GFP were imaged with SDCM with a Z-step of 0.3 μm. A subset of the cross-sectional images is shown at the indicated depth (3, 6, 9, 12, 15, 18 and 21 μm) along with the maximum-intensity projection of all 67 images through epidermis. BIK1-GFP localizes to both PM and endosomal puncta (white arrows) within all sections. **k-p**. Quantification method for BIK1-GFP puncta within maximum-intensity projections of SDCM images. **k**. Maximum-intensity projections (MIP) were generated using Fiji distribution of ImageJ 1.51 (https://fiji.sc/) for each Z-series captured by SDCM imaging of BIK1-GFP cotyledons. **l**. Regions of MIP with non-pavement cells (e.g. stomata) are removed from the image using the Line Draw and Crop functions. The total surface area (μm^2) of the image is measured using the Analyze Measure function. **m**. Puncta within the cropped MIP are recognized using a customized model generated and applied with the Trainable Weka Segmentation plug-in for Fiji. The same model is applied to all images to generate binary images showing the physical location of each BIK1-GFP puncta (black). **n-o**. Puncta within the size range of 0.1–2.5 μm^2 are highlighted in green (n) and counted (o) using the Analyze Particles function in Fiji. BIK1-GFP endocytosis is quantified as the number of puncta per 1000 μm^2. **p**. An overlay of the BIK1-GFP puncta (yellow highlight) over the cropped MIP confirms correct identification of puncta. The experiments in a-c were repeated three times with similar results.

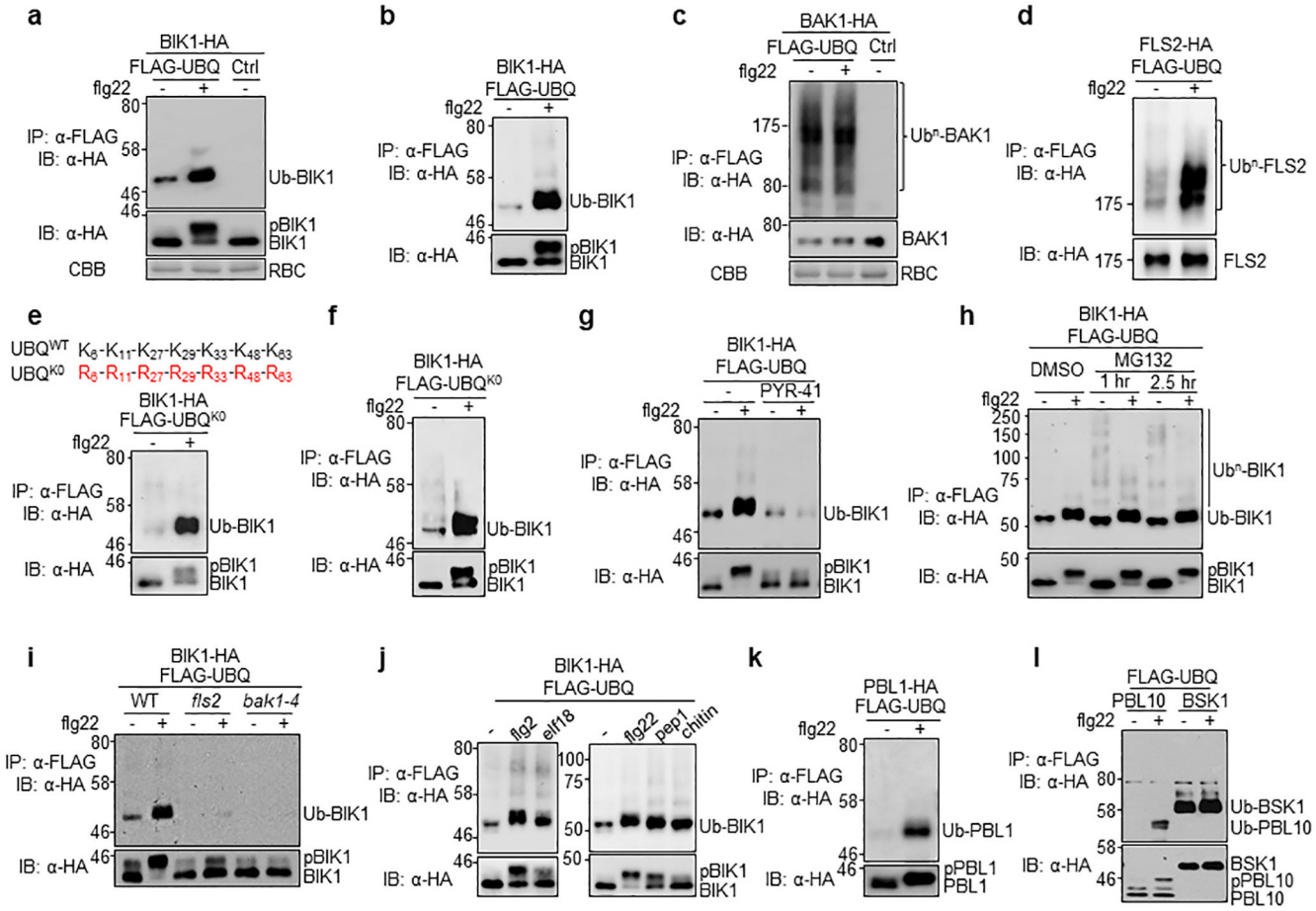

Extended Data Figure 2. MAMP-triggered BIK1 family RLCK monoubiquitination.

a. Flg22 induces monoubiquitination of BIK1. Protoplasts from WT plants were transfected with BIK1-HA and FLAG-UBQ or a vector (Ctrl), and followed by treatment with 100 nM flg22 for 30 min. After IP with α-FLAG, ubiquitinated BIK1 was detected by IB using α-HA antibody (top). The middle panel shows BIK1-HA proteins and the bottom shows Coomassie Brilliant Blue (CBB) staining for RuBisCO (RBC). **b**. Flg22 induces BIK1 monoubiquitination in *pBIK1::BIK1-HA* transgenic plants. Protoplasts from *pBIK1::BIK1-HA/bik1* transgenic plants were transfected with FLAG-UBQ and followed by 100 nM flg22 treatment for 30 min. After IP with α-FLAG agarose, ubiquitinated BIK1 was detected by IB with α-HA antibody (top). The bottom panel shows BIK1-HA proteins. **c**. BAK1 is constitutively polyubiquitinated *in vivo*. Protoplasts from WT plants were transfected with BAK1-HA and FLAG-UBQ or control, and followed by 100 nM flg22 treatment for 30 min. IP was carried out with α-FLAG agarose (IP: α-FLAG). Ubiquitinated BAK1 (Ub-BAK1) proteins were detected as a smear with α-HA IB (IB: α-HA) (Top). The middle panel shows BAK1-HA proteins and the bottom is CBB staining for RBC. **d**. Flg22 induces FLS2 polyubiquitination. Protoplasts from WT plants were transfected with FLS2-HA and FLAG-UBQ and followed by 100 nM flg22 treatment for 30 min. **e, f**. Monoubiquitination of BIK1 with UBQ^{K0}. Protoplasts from *pBIK1::BIK1-HA* (e) or *35S::BIK1-HA* (f) transgenic plants were transfected with FLAG-UBQ^{K0} (all lysine residues mutated to arginine) and followed by 100 nM flg22 treatment for 30 min. The mutations of lysine-to-arginine in UBQ^{K0} are

shown on top with amino-acid positions labeled (e). **g**. PYR-41 blocks flg22-induced BIK1 monoubiquitination. PYR-41 (50 μM) was added 30 min prior to flg22 treatment. **h**. Flg22 induces BIK1 monoubiquitination in the presence of MG132. MG132 (2 μM) was added 1 hr or 2.5 hr before adding flg22. **i**. Flg22-induced BIK1 monoubiquitination depends on FLS2 and BAK1. Protoplasts isolated from WT, *fls2* and *bak1–4* plants were transfected with BIK1-HA and FLAG-UBQ, and followed by treatment with 100 nM flg22 for 30 min. **j**. Elf18, pep1 and chitin induce BIK1 monoubiquitination. 1 μM elf18, 200 nM pep1 or 100 μg/ml chitin was added for 30 min. **k**. BIK1 homolog PBL1 is monoubiquitinated upon flg22 treatment. PBL1-HA and FLAG-UBQ were expressed in protoplasts. **l**. Flg22 induces monoubiquitination of BIK1 family RLCK PBL10, but not BSK1. HA-tagged PBL10 or BSK1 was expressed with FLAG-UBQ in WT protoplasts. The experiments were repeated at least three times with similar results.

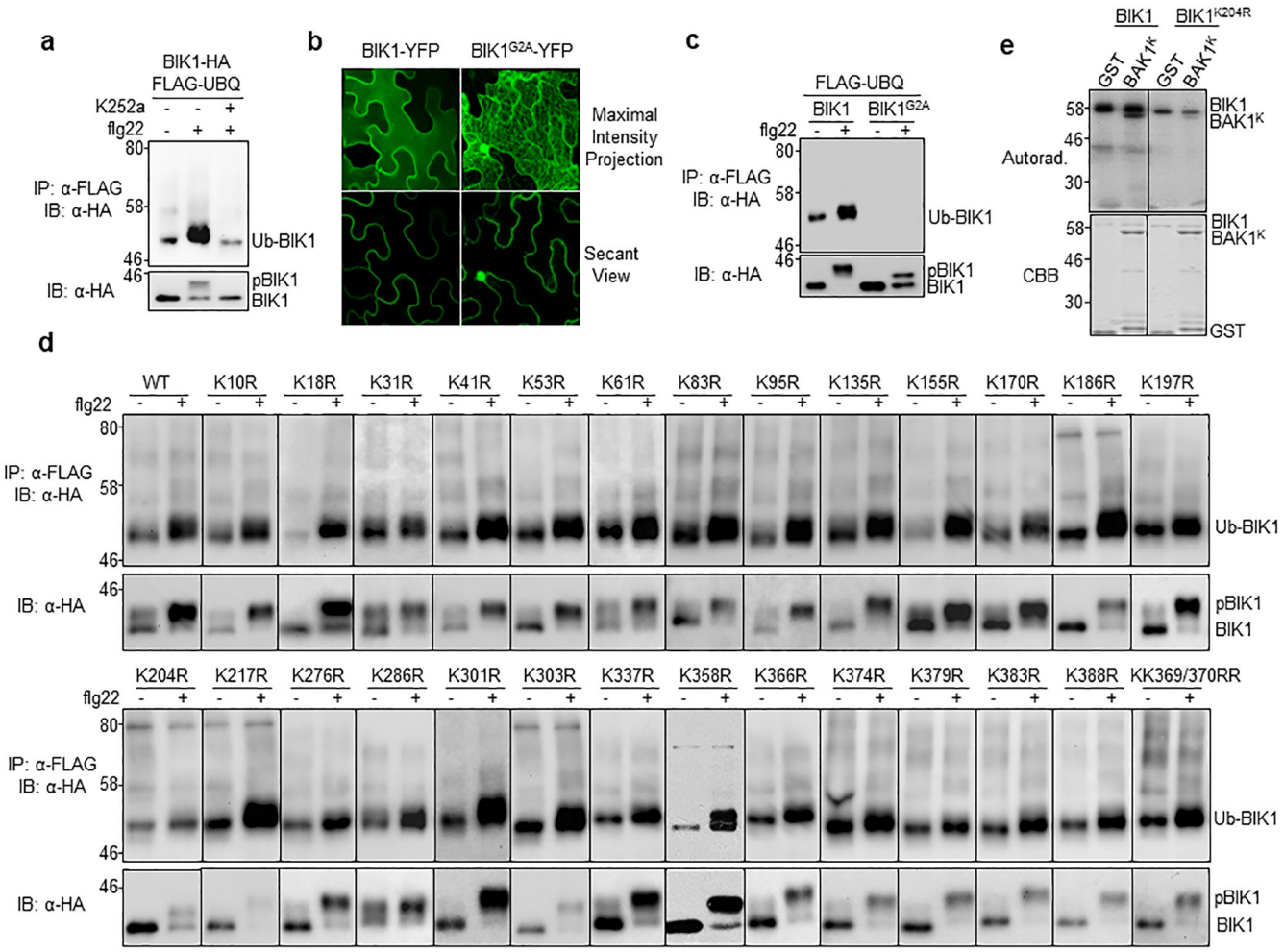

Extended Data Figure 3. Plasma membrane localization and phosphorylation are required for BIK1 ubiquitination.

a. The kinase inhibitor K252a blocks flg22-induced BIK1 ubiquitination. Protoplasts transfected with FLAG-UBQ and BIK1-HA were treated with 1 μM K252a for 30 min prior to 100 nM flg22 treatment. **b**. $BIK1^{G2A}$ no longer localizes to PM. BIK1-YFP or $BIK1^{G2A}$-YFP was expressed in *N. benthamiana* for imaging analysis. **c**. $BIK1^{G2A}$ compromises flg22-induced monoubiquitination. BIK1-HA or $BIK1^{G2A}$-HA was co-expressed with FLAG-UBQ in protoplasts. **d**. Single K-to-R mutations of BIK1 fail to block flg22-induced ubiquitination without altering kinase activity. HA-tagged BIK1 WT or mutants was co-expressed with FLAG-UBQ in protoplasts. **e**. $BIK1^{K204R}$ exhibits reduced autophosphorylation and phosphorylation activity on BAK1. An *in vitro* kinase assay was performed using GST-BIK1 or GST-$BIK1^{K204R}$ as a kinase and GST or GST-$BAK1^{K}$ (BAK1 kinase domain without detectable autophosphorylation activity) as a substrate with [γ-^{32}P] ATP. Proteins were separated with SDS-PAGE and analyzed by autoradiography (Autorad.) (top). Protein loading is shown by CBB staining (bottom). The experiments were repeated at least twice with similar results.

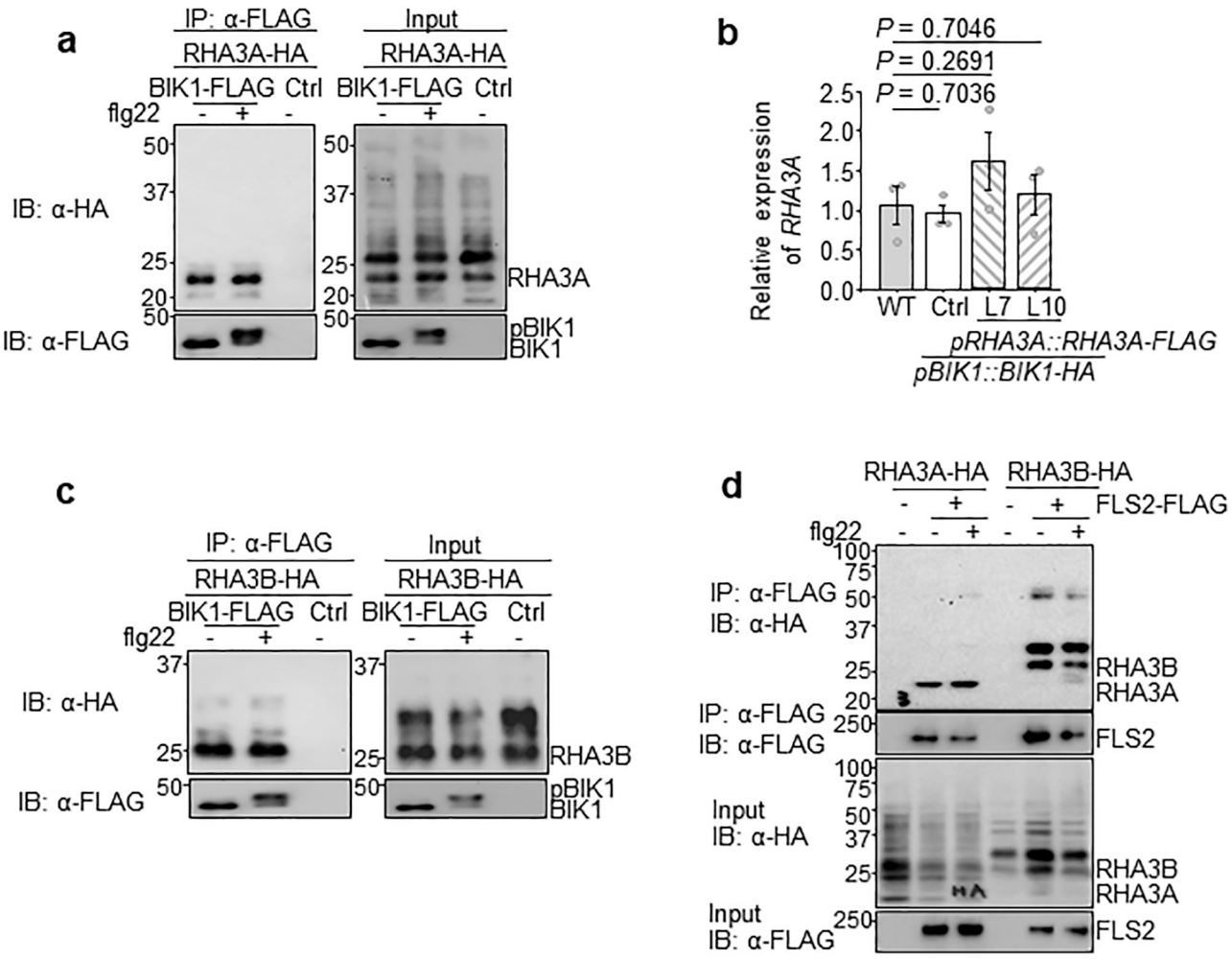

Extended Data Figure 4. RHA3A/B interacts with BIK1 *in vivo*.

a. BIK1 interacts with RHA3A in a Co-IP assay. RHA3A-HA was co-expressed with BIK1-FLAG or Ctrl in protoplasts followed by 100 nM flg22 treatment for 15 min. The Co-IP assay was carried out with α-FLAG agarose and immunoprecipitated proteins were immunoblotted with α-HA or α-FLAG antibody (left). The right panels show BIK1-FLAG and RHA3A-HA proteins. **b**. *RHA3A* expression in *pRHA3A::RHA3A-FLAG/ pBIK1::BIK1-HA* transgenic plants. qRT-PCR was carried out to detect *RHA3A* transcripts using *ACTIN2* as a control. The relative gene expression from WT (set as 1), *pBIK1::BIK1-HA* (Ctrl) and two independent transgenic lines (line 7 and 10) is shown. Data are shown as means ± SEM (One-way ANOVA, n=3). **c**. BIK1 associates with RHA3B independent of flg22 treatment. RHA3B-HA was co-expressed with BIK1-FLAG or Ctrl in protoplasts followed by 100 nM flg22 treatment for 15 min. Co-IP assay was carried out with α-FLAG agarose and immunoprecipitated proteins were immunoblotted with α-HA or α-FLAG antibody (left). Right panels show BIK1-FLAG and RHA3B-HA proteins before IP. **d**. FLS2 interacts with RHA3A and RHA3B in a Co-IP assay. The experiments were repeated three times with similar results.

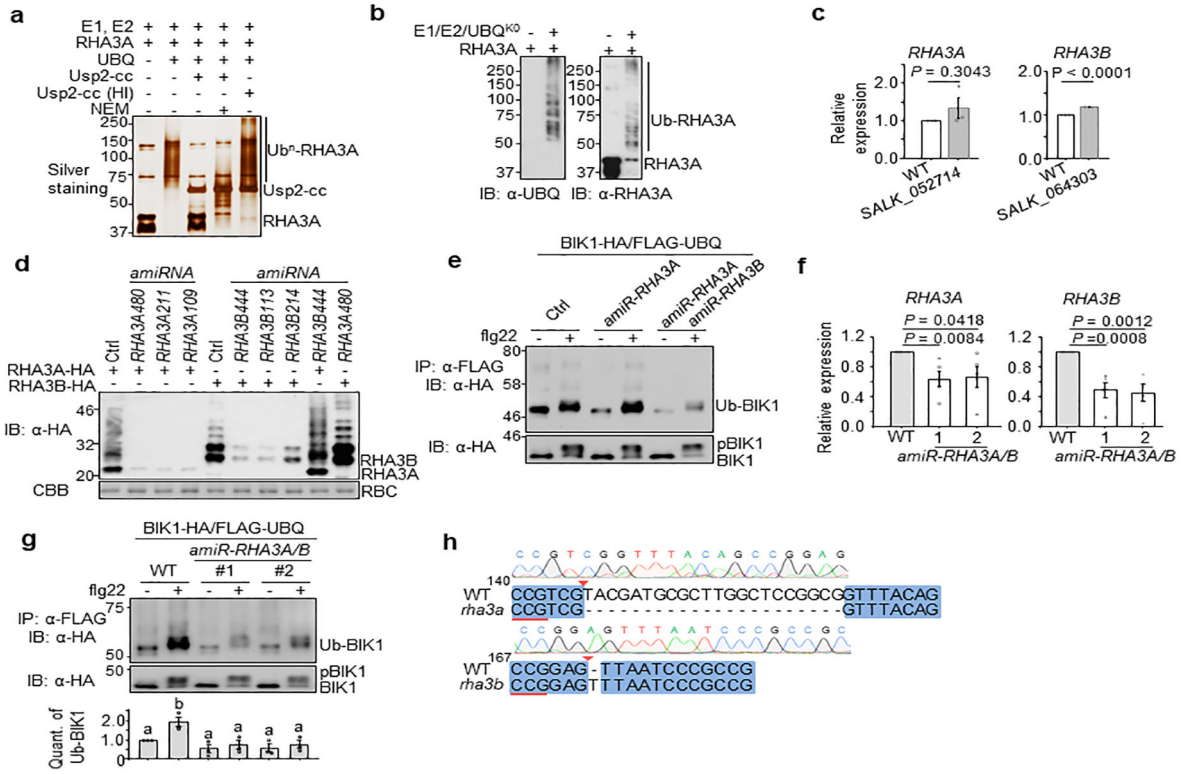

Extended Data Figure 5. RHA3A/B ubiquitinate BIK1 *in vivo*.

a. GST-RHA3A^{CD} possesses E3 ligase activity *in vitro*. The *in vitro* ubiquitination assay was performed with GST-RHA3A^{CD} followed by deubiquitination reactions with GST-Usp2-cc. N-Ethylmaleimide (NEM) (10 mM), an inhibitor of deubiquitinases, and heat-inactivated (HI, 95°C for 5 min) Usp2-cc are controls. Samples were analyzed by SDS-PAGE and silver staining. **b**. GST-RHA3A^{CD} possesses multi-monoubiquitination activity *in vitro*. Ubiquitination assay was done similarly as (a) except using the ubiquitin mutant with all lysine residues mutated to arginine (UBQ^{K0}). Ubiquitinated proteins were detected by IB with α-UBQ (left) or α-RHA3A (right) antibody. **c**. *RHA3* expression in T-DNA insertion mutants. *RHA3A* expression in T-DNA knockout line *SALK_052714* and *RHA3B* expression in *SALK_064303* were analyzed as in Extended Data Fig. 4b. Data are shown as means ± SEM of fold change (WT as 1.0) (Two-tailed Student's *t*-test, *n*=3). **d**. Screen for the optimal *amiR-RHA3A* and *amiR-RHA3B*. Protoplasts were transfected with *RHA3A-HA* or *RHA3B-HA* with Ctrl, *amiR-RHA3A* or *amiR-RHA3B*. RHA3A or RHA3B proteins were examined by IB with α-HA antibody. **e**. RHA3A and RHA3B are required for BIK1 ubiquitination *in vivo*. BIK1 ubiquitination assay was carried out by co-expressing Ctrl, artificial microRNA targeting *RHA3A* (*amiR-RHA3A*) or together with microRNA targeting *RHA3B* (*amiR-RHA3A amiR-RHA3B*). **f**. *RHA3A* and *RHA3B* expression in *amiR-RHA3A/B* transgenic plants. qRT-PCR was carried out to detect *RHA3A* and *RHA3B* transcripts with *ACTIN2* as a control. Fold changes of the gene expression from two independent transgenic lines (line 1 & 2) are shown. Data are shown as means ± SEM (One-way ANOVA, *n*=5). **g**. RHA3A and RHA3B are required for BIK1 ubiquitination in transgenic plants. Protoplasts from *amiR-RHA3A/B* transgenic plants were transfected with

BIK1-HA and FLAG-UBQ for ubiquitination assay. Quantification of BIK1 ubiquitination in *amiR-RHA3A/B* transgenic plants is shown on bottom. Intensity of Ub-BIK1 or BIK1 bands was quantified with Image Lab (Bio-Rad). The amount of BIK1 ubiquitination is the relative intensity of Ub-BIK1 band to BIK1 band (no treatment in WT as 1.0). Data are shown as means ± SEM. Different letters indicate significant difference with others ($P < 0.05$, One-way ANOVA, $n=3$). **h**. Sequencing analysis of *RHA3A* and *RHA3B* genes in the CRISPR/Cas9 *rha3a/b* mutant. PCR fragments corresponding to *RHA3A* and *RHA3B* in *rha3a/b* were amplified, sequenced, and aligned to WT coding sequences. Reverse-complement of the PAM sequence is underlined with red, and arrow indicates the theoretical Cas9 cleavage sites. The experiments were repeated three times with similar results.

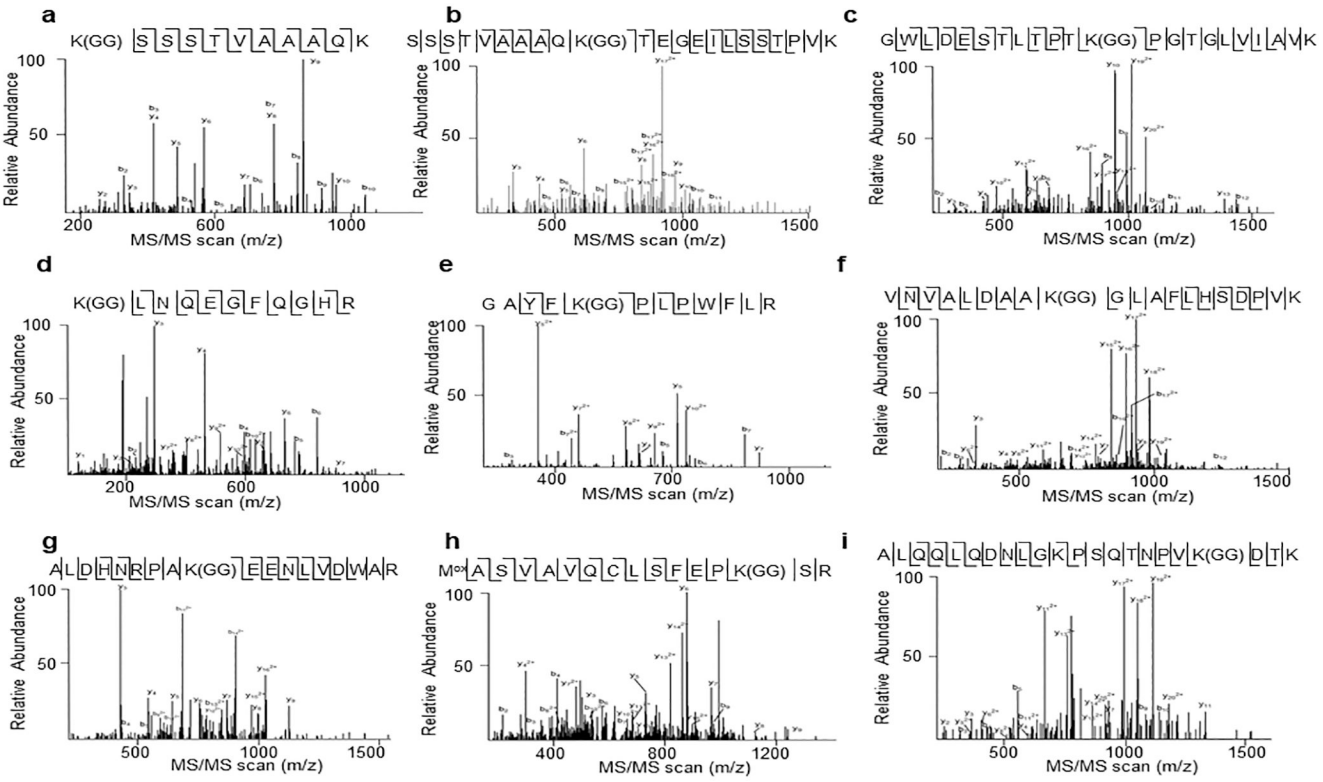

Extended Data Figure 6. BIK1 *in vitro* ubiquitination sites identified by mass spectrometry.

MS/MS spectrums of peptides containing ubiquitinated lysine residues of BIK1 are shown from **a** to **i**. **a**. K31; **b**. K41; **c**. K95; **d**. K106; **e**. K170; **f**. K186; **g**. K286; **h**. K337; **i**. K366. MS spectrums are outputs from the SEQUEST program. MS analysis was performed once.

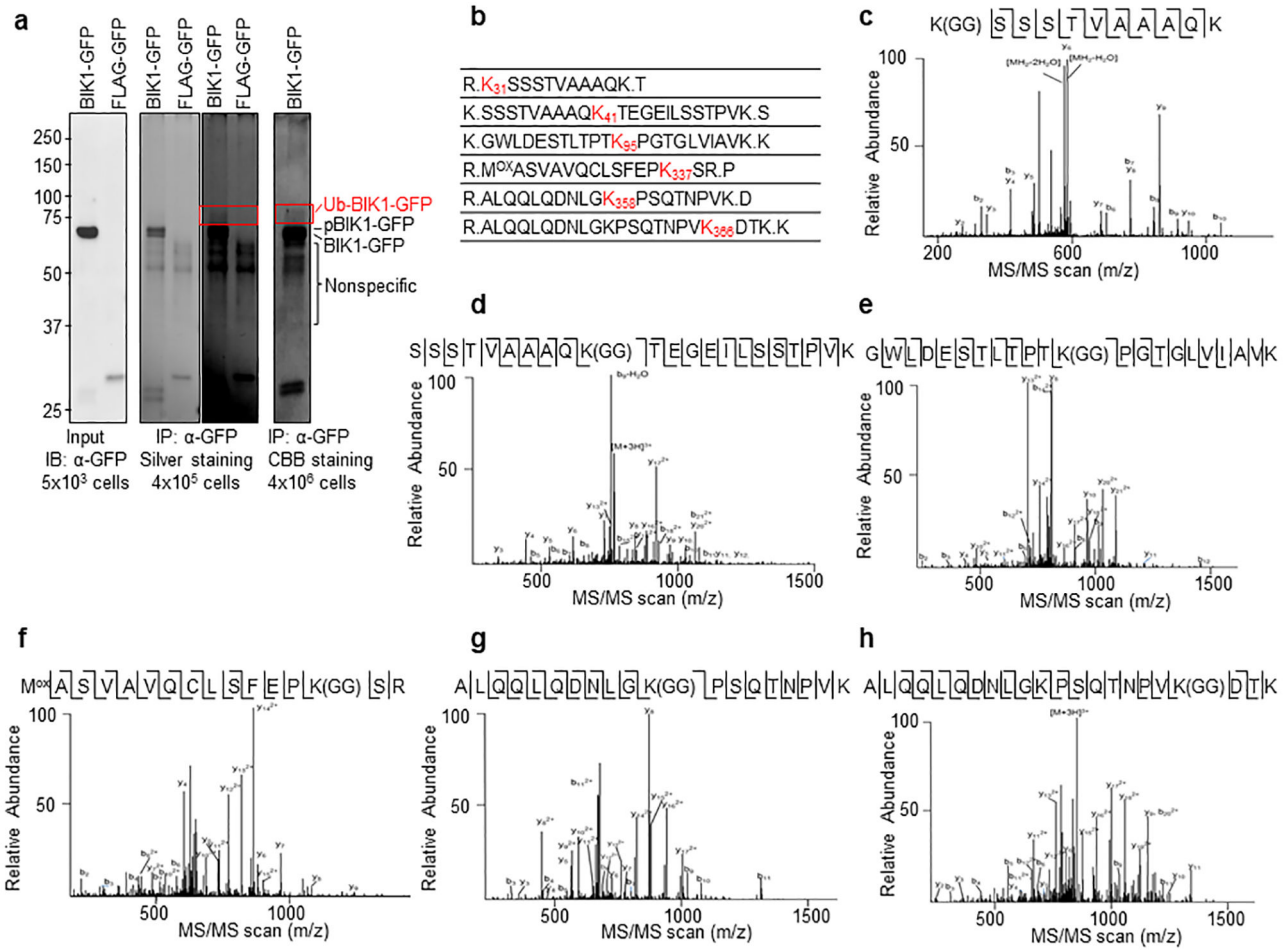

Extended Data Figure 7. BIK1 *in vivo* ubiquitination sites identified by mass spectrometry.

a. Ubiquitinated BIK1-GFP *in planta* was immunoprecipitated for LC-MS/MS analysis. BIK1-GFP and FLAG-UBQ were co-expressed in WT protoplasts (~4 × 10^6 cells) followed by 200 nM flg22 treatment for 30 min. Ubiquitinated BIK1 was immunoprecipitated by GFP-trap-agarose, separated by SDS-PAGE, digested by trypsin and subjected to LC-MS/MS analysis. Portions of cell lysates were examined for BIK1-GFP expression (left), and immunoprecipitates were analyzed by SDS-PAGE following silver staining (middle, right for longer exposure of the same gel) and SDS-PAGE following CBB staining (right). The highlighted area was cut and analyzed by MS. **b**. BIK1 is ubiquitinated *in vivo*. Ubiquitinated lysine containing a diglycine remnant by LC-MS/MS analysis are marked as red with amino acid positions. **c** to **h**. MS/MS spectrums of peptides containing ubiquitinated lysine of BIK1 are shown. **c**. K31; **d**. K41; **e**. K95; **f**. K337; **g**. K358; **h**. K366. MS spectrums are outputs from the SEQUEST program. MS analysis was performed once.

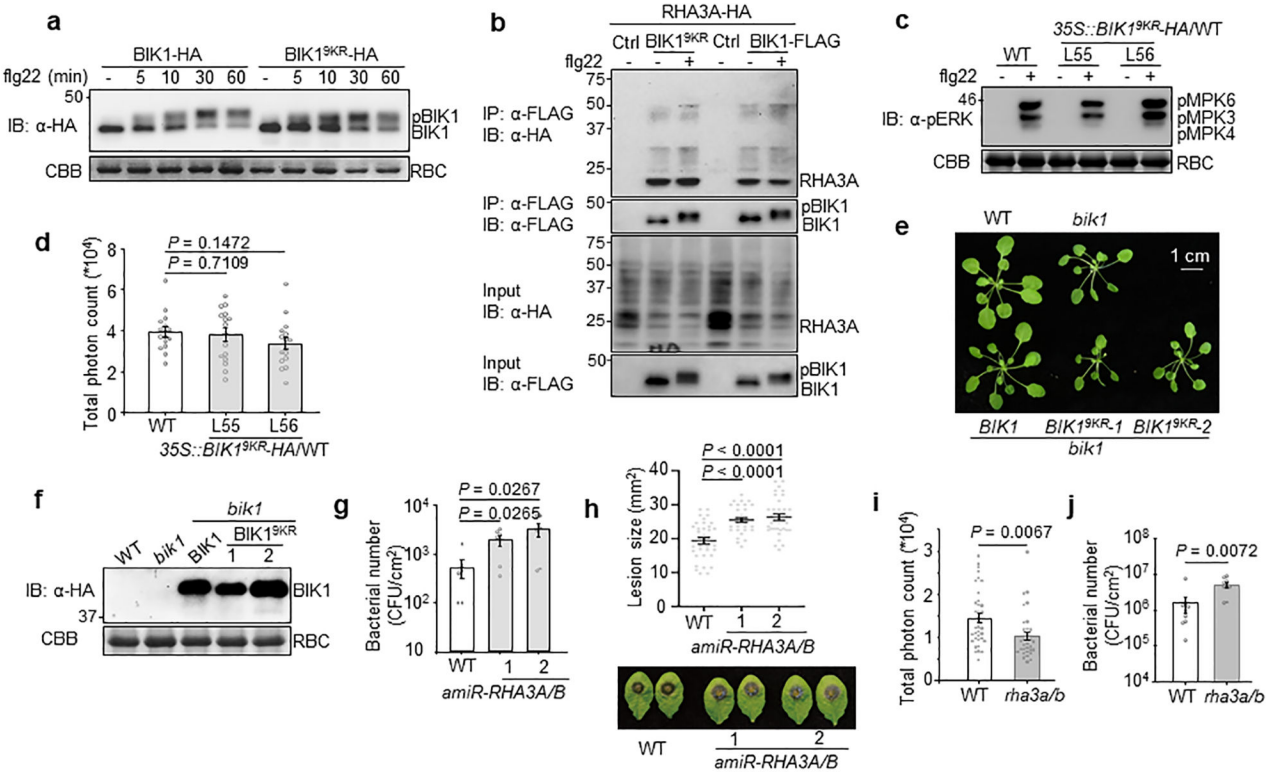

Extended Data Figure 8. BIK1 monoubiquitination is required for plant defense and flg22 signaling.

a. BIK1^{9KR} undergoes phosphorylation similar to BIK1 upon flg22 treatment. BIK1-HA or BIK1^{9KR}-HA was expressed in WT protoplasts followed by 100 nM flg22 treatment for indicated time points. Band-shift of BIK1 was examined by IB with α-HA antibody. **b**. BIK1^{9KR} interacts with RHA3A in a Co-IP assay. RHA3A-HA was co-expressed with BIK1-FLAG or BIK1^{9KR}-FLAG in protoplasts followed by 100 nM flg22 treatment for 15 min. Co-IP assay was carried out with α-FLAG agarose and immunoprecipitated proteins were immunoblotted with α-HA or α-FLAG antibody (top two panels). Bottom two panels show BIK1-FLAG/BIK1^{9KR}-FLAG and RHA3A-HA proteins. **c**. Transgenic plants with *BIK1^{9KR}* overexpression in WT background show similar MAPK activation as WT. Eleven-day-old seedlings of WT or *35S::BIK1^{9KR}-HA*/WT transgenic plants (Line 55 and 56) were treated with 200 nM flg22 for 15 min. MAPK activation was analyzed with α-pERK antibody (top), and protein loading is shown by CBB staining for RBC (bottom). **d**. Transgenic plants with *BIK1^{9KR}* overexpression in WT background show similar flg22-induced ROS production as WT. Leaf discs from the indicated genotypes were treated with 100 nM flg22, and ROS production was measured as relative luminescence units by a luminometer over 50 min. Data are shown as overlay of dot plot and means of total photon count ± SEM (One-way ANOVA, n=16). **e**. Growth phenotype of *pBIK1::BIK1-HA/bik1* and *pBIK1::BIK1^{9KR}-HA/bik1* transgenic plants. Five-week-old soil-grown plants are shown. Scale bar, 1 cm. **f**. Expression of BIK1-HA or BIK1^{9KR}-HA in transgenic plants. Total proteins from leaves of four-week-old transgenic plants were subjected to α-HA IB (top). Bottom panel shows CBB staining for RBC. **g**. RHA3A and RHA3B play a role in disease resistance to *Pst* DC3000 *hrcC*$^-$ infection. Plants were spray-inoculated with *Pst*

DC3000 *hrcC*$^{-}$ and bacterial growth was measured at four days post-inoculation (dpi). Data are shown as overlay of dot plot and means ± SEM (One-way ANOVA, n=6). **h**. RHA3A and RHA3B play a role in disease resistance to *Botrytis*. Four-week-old plant leaves were deposited with 10 μL of *B. cinerea* BO5 at a concentration of 2.5×10^5 spores per mL. Disease symptom was recorded, and the lesion diameter was measured at two dpi. Data are shown as overlay of dot plot and means ± SEM (One-way ANOVA, n=34). **i**. ROS production is reduced in *rha3a/b*. Leaf discs from WT or *rha3a/b* were treated with 100 nM flg22 for ROS production over 50 min. Data are shown as overlay of dot plot and means of total photon count ± SEM (Two-tailed Student's t-test, n=36 for WT and n=32 for *rha3a/b*). **j**. RHA3A and RHA3B play a role in disease resistance to *Pst* DC3000. Plants were spray-inoculated with *Pst* DC3000 and bacterial growth was measured at three dpi. Data are shown as overlay of dot plot and means ± SEM (Two-tailed Student's t-test, n=9). The experiments were repeated three times with similar results.

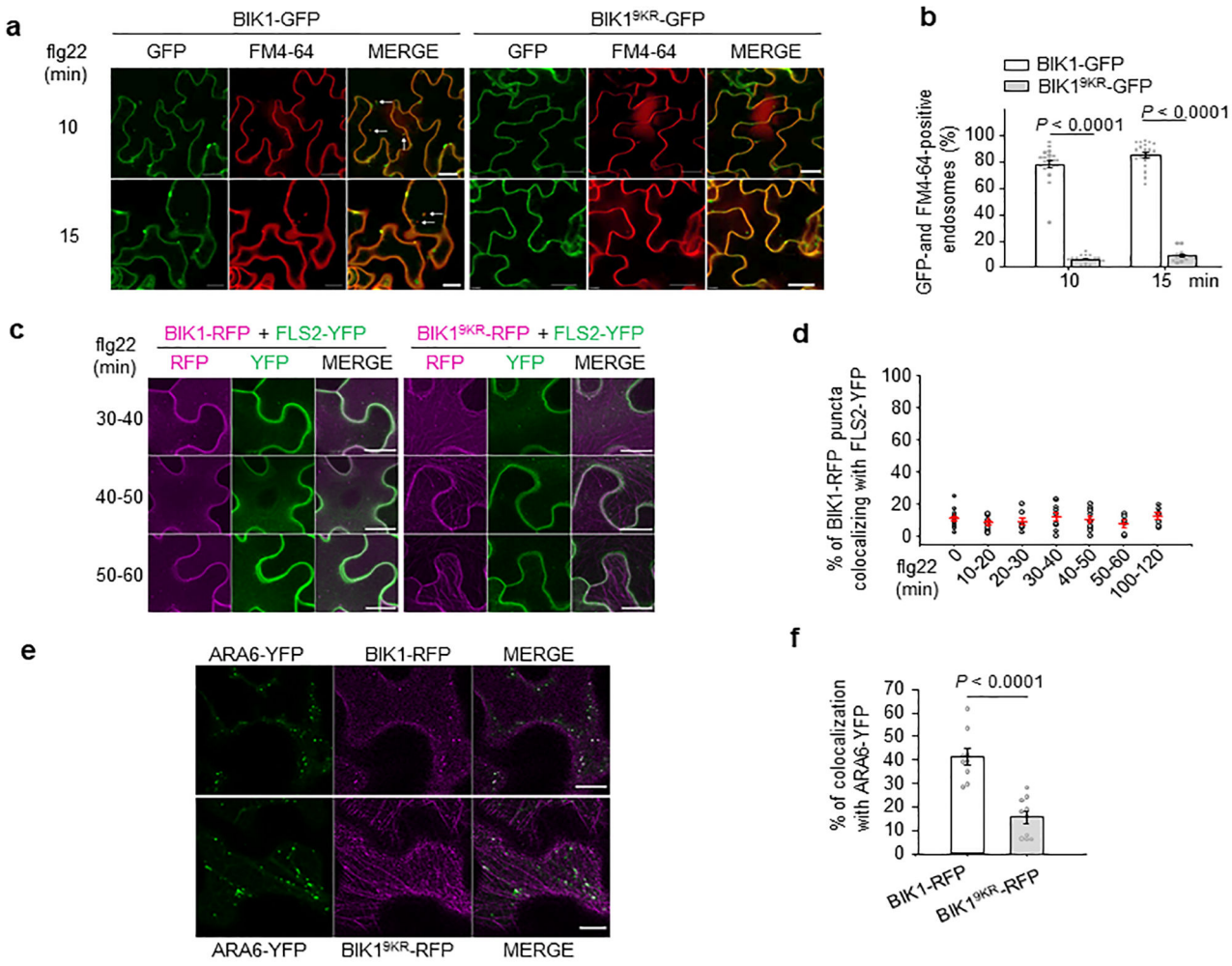

Extended Data Figure 9. The BIK1^{9KR} mutation impairs flg22-induced BIK1 endocytosis.

a. **b**. BIK1^{9KR}-GFP-labelled puncta colocalize less with FM4–64 than BIK1-GFP upon flg22 treatment. Five-day-old seedlings of *35S::BIK1-GFP* or *35S::BIK1^{9KR}-GFP* were pretreated with FM4–64 (2 μM) for 15 min and elicited with 100 nM flg22 for the indicated time points and fluorescence was detected in epidermis by a confocal microscopy (a). White arrow points to colocalized endosomes. Scale bars, 20 μm. Percentage of BIK1-GFP or BIK1^{9KR}-GFP and FM4–64 positive endosomes over time per 100% of image area is shown in (b). Data are shown as overlay of dot plot and means ± SEM (Two-tailed Student's *t*-test, n = 21 images for BIK1-GFP and n= 16, 15 images for 10, 15 min respectively for BIK1^{9KR}-GFP). **c**. Flg22-induced BIK1, BIK1^{9KR} and FLS2 endocytosis in *N. benthamiana*. BIK1-TagRFP (BIK1-RFP) or BIK1^{9KR}-TagRFP (BIK1^{9KR}-RFP) was co-expressed with FLS2-YFP in *N. benthamiana*, infiltrated with 100 μM flg22 and imaged at the indicated time points by a confocal microscopy. The images of 30–40, 40–50 and 50–60 min after flg22 treatment from Fig. 4e are shown here. Scale bars, 20 μm. For BIK1-RFP/FLS2-YFP, n= 14, 11, 7, 10, 10, 6, 7 images for 0, 10–20, 20–30, 30–40, 40–50, 50–60, 100–120 min; for BIK1^{9KR}-RFP/FLS2-YFP, n= 19, 11, 11, 9, 16, 12, 7 images for 0, 10–20, 20–30, 30–40, 40–50, 50–60, 100–120 min respectively. **d**. Percentage of BIK1-RFP puncta colocalizing

with FLS2-YFP after flg22 treatment for the indicated time points in Fig. 4e and Extended Data Fig. 9c. Data are shown as overlay of dot plot and means ± SEM (n= 14, 11, 7, 10, 10, 6, 7 images for 0, 10–20, 20–30, 30–40, 40–50, 50–60, 100–120 min respectively). **e-f** BIK1^{9KR}-RFP shows reduced co-localization with ARA6-YFP. BIK1-RFP or BIK1^{9KR}-RFP was transiently expressed with ARA6-YFP in *N. benthamiana*, and the images were taken 48–72 hr after infiltration (e). Scale bars, 10 μm. Percentage of BIK1-RFP puncta colocalizing with ARA6-YFP is shown in f. Data are shown as overlay of dot plot and means ± SEM (Two-tailed Student's *t*-test, n= 9 images for BIK1-RFP; n= 10 images for BIK1^{9KR}-RFP). The experiments were repeated three times with similar results.

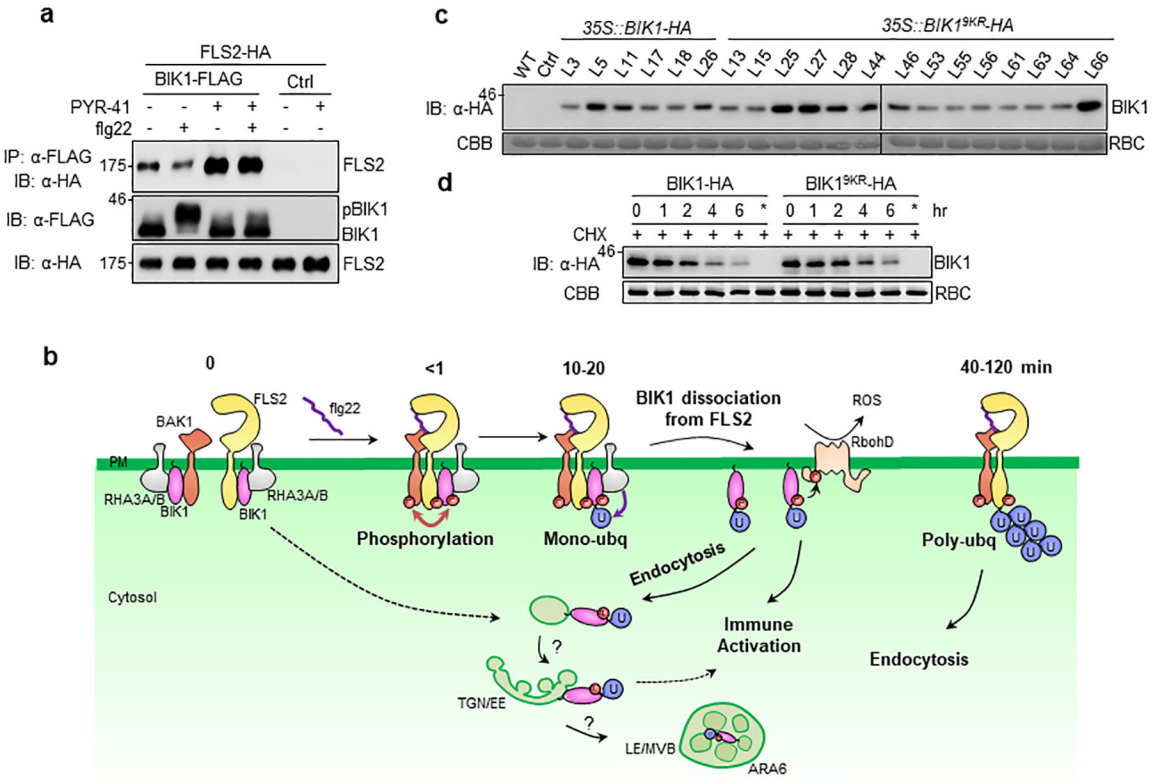

Extended Data Figure 10. Monoubiquitination mediates BIK1 release from PM upon ligand perception.

a. PYR-41 impairs flg22-induced BIK1 dissociation from FLS2. FLS2-HA was co-expressed with BIK1-FLAG or Ctrl in protoplasts. After pretreatment with 50 μM PYR-41 for 30 min, protoplasts were stimulated with 100 nM flg22 for 15 min. Co-IP and IB were performed as in Fig. 4g. **b**. A working model of RHA3A/B-mediated BIK1 monoubiquitination in plant immunity. During non-activated, steady state condition (0 min), BIK1 remains hypo-phosphorylated and associates with FLS2 and BAK1. Upon flg22 perception, FLS2 dimerizes with BAK1, which stimulates BIK1 phosphorylation (<1 min). The phosphorylated BIK1 is monoubiquitinated by E3 ligases RHA3A and RHA3B, leading to BIK1 dissociation from FLS2-BAK1 complex, accompanied by endocytosis (10–20 min). Ligand-induced BIK1 monoubiquitination contributes to the activation of ROS and other defense responses. FLS2 is polyubiquitinated and endocytosed 40 min after flg22 perception for signaling attenuation. **c**. BIK1^{9KR} shows comparable protein level as BIK1 in transgenic plants. *35S::BIK1-HA* or *35S::BIK1^{9KR}-HA* transgenic plants in WT background were used for IB detecting BIK1 proteins by α-HA antibody. Ctrl is empty vector transgenic plants. **d**. BIK1 and BIK1^{9KR} protein stability after cycloheximide treatment. BIK1-HA or BIK1^{9KR}-HA was expressed in WT protoplasts for 12 hr followed by 500 μg/ml cycloheximide (CHX) treatment for the indicated time. BIK1 or BIK1^{9KR} proteins were analyzed by IB with α-HA antibody. * indicates CHX was added right after transfection, thus blocking protein synthesis. The experiments were repeated three times with similar results.

Supplementary Material

Refer to Web version on PubMed Central for supplementary material.

Acknowledgements

We thank Dr. Qijun Chen (China Agricultural University, China) for the CRISPR/Cas9 system, Drs. Jianfeng Li (Sun Yat-Sen University, China) and Jen Sheen (Harvard Medical School, USA) for the amiRNA system, Dr. Paul de Figueiredo (Texas A&M University, USA) for mouse cDNA, Drs. Timothy Devarenne, Martin Dickman, Craig Kaplan and Tatyana Igumenova (Texas A&M University, USA), and the members in Shan and He laboratories for discussion and comments on this work. The work was supported by NIH (R01GM097247) and the Robert A. Welch foundation (A-1795) to L.S., National Science Foundation (NSF) (MCB-1906060) and NIH (R01GM092893) to P.H, NSF (IOS-1147032) to A.H, the Special Research Fund (BOF15/24J/048) to E. R., and NIH (R01GM114260) to J.P. The authors have declared no conflict of interests.

References

1. Couto D & Zipfel C Regulation of pattern recognition receptor signalling in plants. Nat Rev Immunol 16, 537–552, (2016). [PubMed: 27477127]
2. Yu X, Feng B, He P & Shan L From Chaos to Harmony: Responses and Signaling upon Microbial Pattern Recognition. Annu Rev Phytopathol 55, 109–137, (2017). [PubMed: 28525309]
3. Spoel SH & Dong X How do plants achieve immunity? Defence without specialized immune cells. Nat Rev Immunol 12, 89–100, (2012). [PubMed: 22273771]
4. Liang X & Zhou JM Receptor-Like Cytoplasmic Kinases: Central Players in Plant Receptor Kinase-Mediated Signaling. Annu Rev Plant Biol 69, 267–299, (2018). [PubMed: 29719165]
5. Lu D et al. A receptor-like cytoplasmic kinase, BIK1, associates with a flagellin receptor complex to initiate plant innate immunity. Proc Natl Acad Sci U S A 107, 496–501, (2010). [PubMed: 20018686]
6. Zhang J et al. Receptor-like cytoplasmic kinases integrate signaling from multiple plant immune receptors and are targeted by a Pseudomonas syringae effector. Cell Host Microbe 7, 290–301, (2010). [PubMed: 20413097]
7. Lin W et al. Tyrosine phosphorylation of protein kinase complex BAK1/BIK1 mediates Arabidopsis innate immunity. Proc Natl Acad Sci U S A 111, 3632–3637, (2014). [PubMed: 24532660]
8. Li L et al. The FLS2-associated kinase BIK1 directly phosphorylates the NADPH oxidase RbohD to control plant immunity. Cell Host Microbe 15, 329–338, (2014). [PubMed: 24629339]
9. Kadota Y et al. Direct regulation of the NADPH oxidase RBOHD by the PRR-associated kinase BIK1 during plant immunity. Mol Cell 54, 43–55, (2014). [PubMed: 24630626]
10. Tian W et al. A calmodulin-gated calcium channel links pathogen patterns to plant immunity. Nature 572, 131–135, (2019). [PubMed: 31316205]
11. Smith JM et al. Loss of Arabidopsis thaliana Dynamin-Related Protein 2B reveals separation of innate immune signaling pathways. PLoS Pathog 10, e1004578, (2014). [PubMed: 25521759]
12. Beck M, Zhou J, Faulkner C, MacLean D & Robatzek S Spatio-temporal cellular dynamics of the Arabidopsis flagellin receptor reveal activation status-dependent endosomal sorting. Plant Cell 24, 4205–4219, (2012). [PubMed: 23085733]
13. Robatzek S, Chinchilla D & Boller T Ligand-induced endocytosis of the pattern recognition receptor FLS2 in Arabidopsis. Genes Dev 20, 537–542, (2006). [PubMed: 16510871]
14. Smith JM, Salamango DJ, Leslie ME, Collins CA & Heese A Sensitivity to Flg22 Is Modulated by Ligand-Induced Degradation and de Novo Synthesis of the Endogenous Flagellin-Receptor FLAGELLIN-SENSING2. Plant Physiology 164, 440–454, (2014). [PubMed: 24220680]
15. Lu DP et al. Direct Ubiquitination of Pattern Recognition Receptor FLS2 Attenuates Plant Innate Immunity. Science 332, 1439–1442, (2011). [PubMed: 21680842]
16. Zhou J et al. The dominant negative ARM domain uncovers multiple functions of PUB13 in Arabidopsis immunity, flowering, and senescence. J Exp Bot 66, 3353–3366, (2015). [PubMed: 25873653]

17. Zhou J et al. Regulation of Arabidopsis brassinosteroid receptor BRI1 endocytosis and degradation by plant U-box PUB12/PUB13-mediated ubiquitination. Proc Natl Acad Sci U S A 115, E1906–E1915, (2018). [PubMed: 29432171]
18. Li JF, Zhang D & Sheen J Epitope-tagged protein-based artificial miRNA screens for optimized gene silencing in plants. Nat Protoc 9, 939–949, (2014). [PubMed: 24675734]
19. Lal NK et al. The Receptor-like Cytoplasmic Kinase BIK1 Localizes to the Nucleus and Regulates Defense Hormone Expression during Plant Innate Immunity. Cell Host Microbe 23, 485–497 e485, (2018). [PubMed: 29649442]
20. Ueda T, Yamaguchi M, Uchimiya H & Nakano A Ara6, a plant-unique novel type Rab GTPase, functions in the endocytic pathway of Arabidopsis thaliana. EMBO J 20, 4730–4741, (2001). [PubMed: 11532937]
21. Lin W et al. Inverse modulation of plant immune and brassinosteroid signaling pathways by the receptor-like cytoplasmic kinase BIK1. Proc Natl Acad Sci U S A 110, 12114–12119, (2013). [PubMed: 23818580]
22. Lin W, Ma X, Shan L & He P Big roles of small kinases: the complex functions of receptor-like cytoplasmic kinases in plant immunity and development. J Integr Plant Biol 55, 1188–1197, (2013). [PubMed: 23710768]
23. Wang J et al. A Regulatory Module Controlling Homeostasis of a Plant Immune Kinase. Mol Cell 69, 493–504 e496, (2018). [PubMed: 29358080]
24. Zhou B & Zeng L Conventional and unconventional ubiquitination in plant immunity. Mol Plant Pathol 18, 1313–1330, (2017). [PubMed: 27925369]
25. Wang ZP et al. Egg cell-specific promoter-controlled CRISPR/Cas9 efficiently generates homozygous mutants for multiple target genes in Arabidopsis in a single generation. Genome Biol 16, 144, (2015). [PubMed: 26193878]
26. Tao K, Waletich JR, Arredondo F & Tyler BM Manipulating Endoplasmic Reticulum-Plasma Membrane Tethering in Plants Through Fluorescent Protein Complementation. Frontiers in plant science 10, 635, (2019). [PubMed: 31191568]
27. He P, Shan L & Sheen J The use of protoplasts to study innate immune responses. Methods Mol Biol 354, 1–9, (2007). [PubMed: 17172739]
28. Zhou J, He P & Shan L Ubiquitination of plant immune receptors. Methods Mol Biol 1209, 219–231, (2014). [PubMed: 25117287]
29. Hospenthal MK, Mevissen TET & Komander D Deubiquitinase-based analysis of ubiquitin chain architecture using Ubiquitin Chain Restriction (UbiCRest). Nature Protocols 10, 349–361, (2015). [PubMed: 25633630]
30. Xu P et al. Quantitative proteomics reveals the function of unconventional ubiquitin chains in proteasomal degradation. Cell 137, 133–145, (2009). [PubMed: 19345192]
31. Leslie ME & Heese A Quantitative Analysis of Ligand-Induced Endocytosis of FLAGELLIN-SENSING 2 Using Automated Image Segmentation. Plant Pattern Recognition Receptors: Methods and Protocols 1578, 39–54, (2017).
32. Boruc J et al. Functional modules in the Arabidopsis core cell cycle binary protein-protein interaction network. Plant Cell 22, 1264–1280, (2010). [PubMed: 20407024]

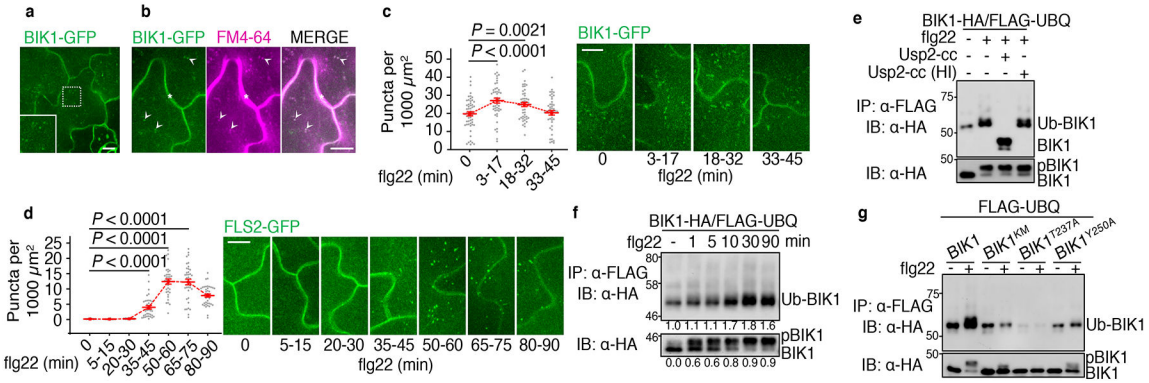

Figure 1. MAMP-induced BIK1 endocytosis and monoubiquitination.

a. BIK1-GFP localizes to cell periphery and intracellular puncta (zoom insert) in maximum intensity projections of cotyledon epidermal cells. Scale bar, 10 μm. **b**. BIK1-GFP colocalizes with FM4–64 in PM (star) and intracellular puncta (arrowheads). Scale bar, 5 μm. BIK1-GFP/FM4–64 Pearson's correlation coefficient = 0.55 ± 0.14 (*n*=35). **c-d**. BIK1 and FLS2 puncta increase after 1 μM flg22 treatment. Data are shown as overlay of dot plot and means ± SEM. *n*=56, 48, 49, 47 images for 0, 3–17, 18–32, 33–45 min respectively for BIK1-GFP (c) and *n*=24, 15, 21, 36, 34, 39, 39 images for 0, 5–15, 20–30, 35–45, 50–60, 65–75, 80–90 min respectively for FLS2-GFP (d). Scale bar, 5 μm. **e**. Flg22 induces BIK1 monoubiquitination. Protoplasts from WT plants were transfected with BIK1-HA and FLAG-UBQ, and treated with 100 nM flg22 for 30 min. After IP with α-FLAG agarose (IP: α-FLAG), ubiquitinated BIK1 was detected by immunoblot (IB) using α-HA antibody (IB: α-HA) (Lane 1 & 2) or with GST-Usp2-cc treatment (Lane 3). Heat inactivated (HI) Usp2-cc is a control (Lane 4). Bottom panel shows BIK1-HA protein expression. Molecular weight (kDa) was labeled on the left of all immunoblots. **f**. Time course of flg22-induced BIK1 phosphorylation and ubiquitination. Protoplasts expressing FLAG-UBQ and BIK1-HA were treated with 100 nM flg22 for the indicated time. BIK1 band intensities were quantified with Image Lab (Bio-Rad). Quantification of BIK1 phosphorylation (underneath bottom panel) is the ratio of intensities of the upper bands (pBIK1) to the sum intensities of shifted and non-shifted bands (pBIK1+BIK1). Quantification of BIK1 ubiquitination (underneath upper panel) is the relative intensity (fold change) of Ub-BIK1 bands (no treatment as 1.0). **g**. BIK1 variants with impaired phosphorylation compromise flg22-induced ubiquitination. All experiments were repeated at least three times with similar results.

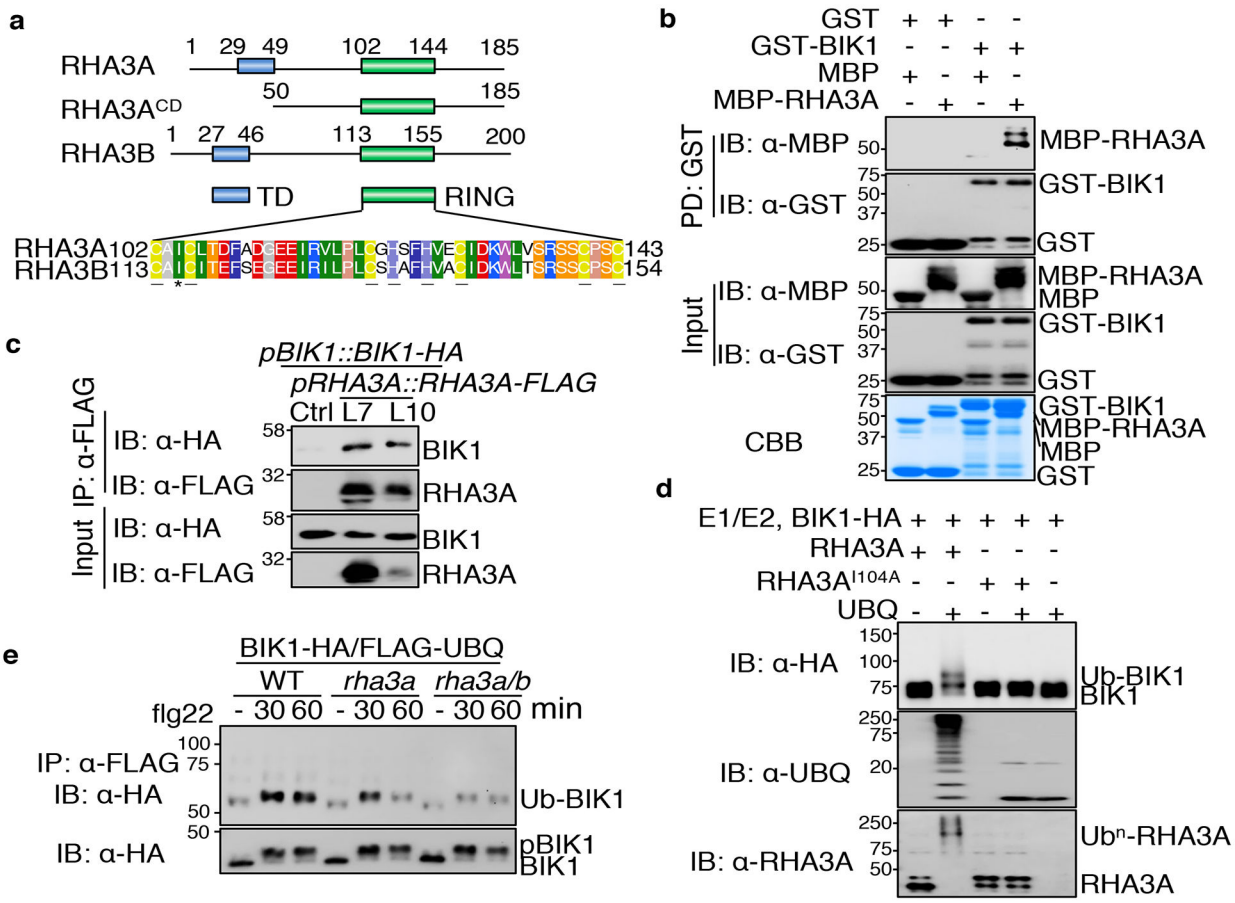

Figure 2. E3 ligases RHA3A/B interact with and monoubiquitinate BIK1.

a. Domain organization of RHA3A/B. TD: transmembrane domain; RING: E3 catalytic domain; RHA3A^{CD}: cytoplasmic domain. Amino acid positions and the sequence of RING domain are shown. Cysteine (C) and histidine (H) residues which coordinate zinc are underlined. Isoleucine (I) involved in E2-RING interaction is labeled with *. **b**. BIK1 interacts with RHA3A. GST or GST-BIK1 proteins immobilized on glutathione sepharose beads were incubated with MBP or MBP-RHA3A^{CD}-HA proteins. Washed beads were subjected to IB with α-MBP or α-GST (top two panels). Input proteins are shown by IB (middle two panels) and Coomassie Brilliant Blue (CBB) staining (bottom). **c**. BIK1 associates with RHA3A. Transgenic plants carrying *pBIK1::BIK1-HA* and *pRHA3A::RHA3A-FLAG* (Line 7 and 10) were used for Co-IP assay with α-FLAG agarose and immunoprecipitated proteins were immunoblotted with α-HA or α-FLAG (top two panels). Bottom two panels show BIK1-HA and RHA3A-FLAG expression. **d**. RHA3A ubiquitinates BIK1. GST-RHA3A^{CD} or its I104A mutant was used in the ubiquitination reaction containing GST-BIK1-HA, E1, E2, and ATP. **e**. RHA3A/B are required for BIK1 ubiquitination. The *rha3a/b* and *rha3a* plants were used for protoplast isolation followed by transfection of BIK1-HA and FLAG-UBQ. The experiments were repeated three times with similar results.

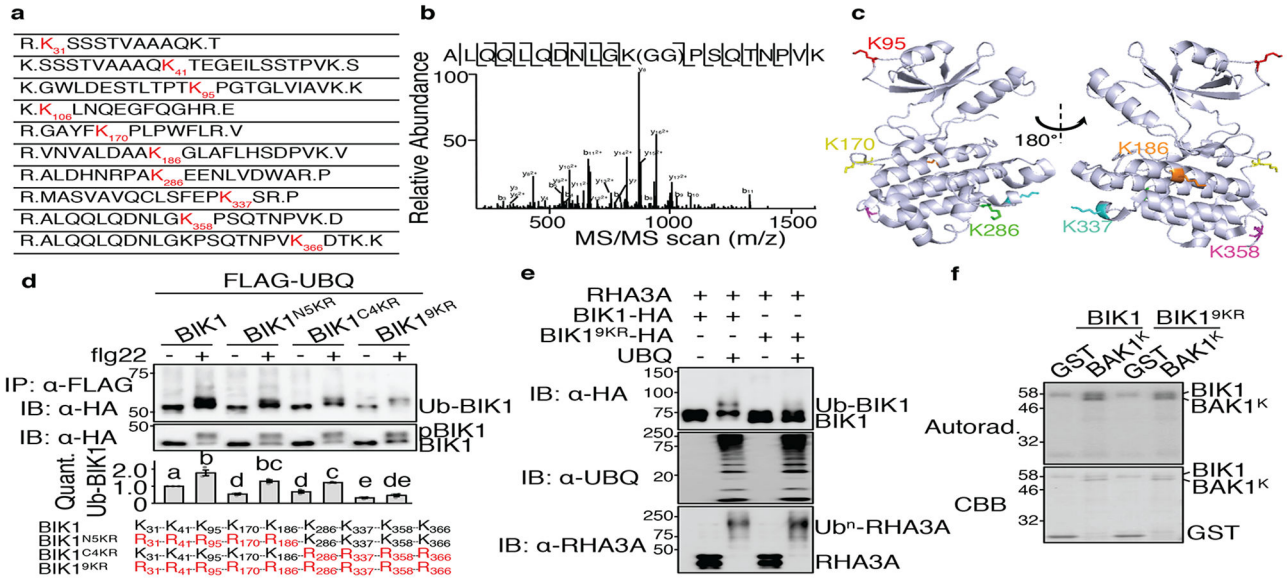

Figure 3. Identification of RHA3A-mediated BIK1 ubiquitination sites.

a. BIK1 is ubiquitinated by RHA3A at multiple lysine residues. Ubiquitinated lysine residues with a diglycine remnant by LC-MS/MS analysis are marked as red with amino acid positions. **b**. MS/MS spectrum of the peptide containing K^{358} is shown. **c**. Structure of BIK1 labeled with six lysine identified as ubiquitination sites. Structural information was obtained from protein data bank (PDB ID: 5TOS) and analyzed by PyMOL. **d**. $BIK1^{9KR}$ is compromised in flg22-induced ubiquitination. FLAG-UBQ and HA-tagged BIK1 mutants were expressed in protoplasts followed by 100 nM flg22 for 30 min. Quantification of BIK1 ubiquitination fold change is shown as overlay of dot plot and means ± SEM (middle). Different letters indicate significant difference with others ($P<0.05$, One-way ANOVA, $n=3$). Mutated lysine for BIK1 mutants are in red (bottom). **e**. RHA3A is unable to ubiquitinate $BIK1^{9KR}$. The assay was performed as in Fig. 2d. **f**. $BIK1^{9KR}$ exhibits normal *in vitro* kinase activity. The kinase assay was performed using GST-BIK1 or GST-$BIK1^{9KR}$ as the kinase and GST or GST-$BAK1^{K}$ (kinase domain) as the substrate. The experiments except MS analyses were repeated three times with similar results.

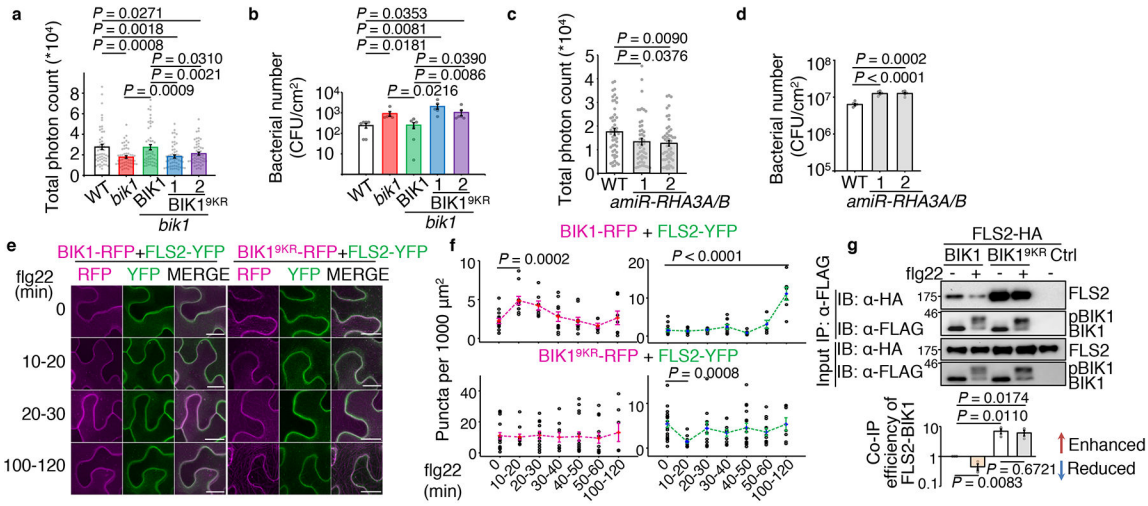

Figure 4. RHA3A/B-mediated BIK1 monoubiquitination contributes to its function in immunity and endocytosis.

a. The *pBIK1::BIK1*^{9KR}*-HA*/*bik1* transgenic plants (Line 1 & 2) cannot complement *bik1* for flg22-induced ROS production. Data are shown as overlay of dot plot and means of total photon count ± SEM (One-way ANOVA, WT, BIK1/*bik1*: *n*=53; *bik1*: *n*=54; BIK1^{9KR}/*bik1*: *n*=55). In all panels, data are shown as overlay of dot plot and means ± SEM, lines beneath p values indicate relevant pair-wise comparisons. **b**. The *pBIK1::BIK1*^{9KR}*-HA*/*bik1* transgenic plants show increased bacterial growth of *Pst* DC3000 *hrcC*$^{-}$. Plants were spray-inoculated and bacterial growth was measured at four days post-inoculation (dpi). One-way ANOVA, *n*=6. **c**. The *amiRNA-RHA3A/B* plants show reduced flg22-induced ROS production. One-way ANOVA, *n*=51. **d**. The *amiRNA-RHA3A/B* plants show increased bacterial growth of *Pst* DC3000. Plants were hand-inoculated and bacterial growth was measured at two dpi. One-way ANOVA, *n*=5. **e**. **f**. Flg22-induced BIK1, BIK1^{9KR}, and FLS2 endocytosis in *N. benthamiana* leaf epidermal cells. BIK1-TagRFP or BIK1^{9KR}-TagRFP was co-expressed with FLS2-YFP followed by 100 μM flg22 treatment and imaged at the indicated time points by a confocal microscopy (e). Scale bars, 20 μm. Quantification of BIK1-TagRFP (magenta) and FLS2-YFP (green) puncta is shown in (f). One-way ANOVA, additional images and *n* values are shown in Extended Data Fig. 9c. **g**. BIK1^{9KR} does not enable flg22-induced BIK1 dissociation from FLS2. Co-IP was performed using protoplasts expressing FLS2-HA and BIK1-FLAG, or BIK1^{9KR}-FLAG, followed by 1 μM flg22 treatment for 15 min (top). BIK1 interaction with FLS2 was quantified as intensity from IP: α-FLAG, IB: α-HA divided by intensity from IP: α-FLAG, IB: α-FLAG (bottom). Data are shown as means ± SEM of fold change (no treatment as 1.0) (One-way ANOVA, *n*=3). All experiments were repeated three times with similar results.